

A UNIVERSAL STRUCTURAL AND STAR-FORMING RELATION SINCE $Z \sim 3$: CONNECTING COMPACT STAR-FORMING AND QUIESCENT GALAXIES

GUILLERMO BARRO^{1,2}, SANDRA M. FABER¹, DAVID C. KOO¹, AVISHAI DEKEL³, JEROME J. FANG¹, JONATHAN R. TRUMP^{4,5}, PABLO G. PÉREZ-GONZÁLEZ⁶, CAMILLA PACIFICI⁷, JOEL R. PRIMACK⁸, RACHEL S. SOMERVILLE⁹, HAOJING YAN¹⁰, YICHENG GUO¹, FENGSHAN LIU¹¹, DANIEL CEVERINO¹², DALE D. KOCEVSKI¹³, ELIZABETH MCGRATH¹³

Last edited: April 5, 2024

ABSTRACT

We study the evolution of the core ($r < 1$ kpc) and effective ($r < r_e$) stellar-mass surface densities (Σ_1 and Σ_e) in star-forming (SFGs) and quiescent galaxies. As early as $z = 3$, both populations occupy distinct linear relations in $\log \Sigma_e$ and $\log \Sigma_1$ vs. $\log M_*$. These structural relations exhibit almost constant slopes and scatter while their normalizations decline with time. For SFGs, the normalization in Σ_e and Σ_1 declines by a factor of ~ 2 since $z = 3$. Such mild declines suggest that SFGs build dense cores by moving *along* these relations. We define this evolution as the *structural main sequence* (Σ -MS), analogous to the star-formation rate main sequence (SFR-MS). Quiescent galaxies follow different relations (Σ_e^q , Σ_1^q) off the Σ -MS by having higher densities than SFGs of the same mass and redshift. The normalization of Σ_e^q declines by a factor of 10 since $z = 3$, while only a factor of ~ 2 in Σ_1^q . Thus, a dense stellar core is present in quiescent galaxies at all redshifts and the formation of such core in SFGs is the main requirement for quenching star-formation. Expressed in 2D as deviations off the SFR-MS and off Σ_1^q at each redshift, the distribution of massive ($\log(M/M_\odot) > 10.3$) galaxies forms a *universal*, L-shaped track that relates two fundamental physical processes: compaction and quenching. Compaction is a process of substantial core-growth in SFGs relative to the evolution in the Σ -MS. This process increases the core-to-total mass and Sérsic index, thereby, making “compact” SFGs structurally similar to quiescent galaxies. Quenching occurs once compact SFGs reach a maximum central density above $\Sigma_1^q \equiv \Sigma_1 - 0.65 \log(M_* - 10.5) \gtrsim 9.5 M_\odot/\text{kpc}^2$. This threshold provides the most effective selection criterion to identify the star-forming progenitors of quiescent galaxies at all redshifts.

Subject headings: galaxies: photometry — galaxies: high-redshift

1. INTRODUCTION

Studies of galaxy evolution from the peak of cosmic star formation to the present day have matured tremendously over the past two decades. The advent of large multi-wavelength photometric surveys have enabled inferences of the global stellar population properties such as stellar mass, age, and star formation rate (SFR). Large-area surveys such as Sloan Digital Sky Survey (SDSS), NMBS, zCOSMOS, UltraVISTA, and zFOURGE have robustly established the shape and evolution of the mass function of star-forming galaxies (SFGs) and quiescent galaxies since $z \sim 4$, cementing our understanding of galaxy build up and shut-down (Peng et al. 2010; Brammer et al. 2011; Ilbert et al. 2013; Muzzin et al. 2013; Woo et al. 2013; Tomczak et al. 2013). Furthermore, the sensitivity and high spatial resolution of *Hubble Space Telescope* (HST) have extended those mass functions further back in cos-

mic time (Bouwens et al. 2010; Finkelstein et al. 2013; Oesch et al. 2014), and have made a pivotal contribution to the study of galaxy sizes and morphologies (e.g., van der Wel et al. 2012; Shibuya et al. 2015). Deep multi-band surveys with HST, such as GOODS (Giavalisco et al. 2004) and CANDELS (Grogin et al. 2011; Koekemoer et al. 2011) have thus provided an exquisite dataset to quantify the simultaneous evolution of the galaxy stellar populations and structural properties across cosmic time.

The consensus is that strong correlations between structure and stellar populations (i.e., a Hubble sequence) exist up to $z = 4$ (Franx et al. 2008; Kriek et al. 2009a; Wuyts et al. 2011a). One such relation is the star formation rate (SFR) main sequence (SFR-MS) (Noeske et al. 2007; Elbaz et al. 2007; Salim et al. 2007; Pannella et al. 2009; Magdis et al. 2010; Wuyts et al. 2011a; Elbaz et al. 2011; Rodighiero et al. 2010; Whitaker et al. 2012; Pannella et al. 2014), which is thought to describe a relatively smooth mode of galaxy growth (Elbaz et al. 2007; Rodighiero et al. 2010) in which gas inflow and SFR have reached a steady-state phase (e.g., Dekel et al. 2013). SFGs on the SFR-MS typically have larger sizes and exponential disk profiles, while quiescent galaxies of the same mass have more concentrated mass profiles (higher Sérsic indices) and smaller sizes. A dichotomy is also present in the size-mass relations, where quiescent galaxies exhibit a much steeper slope than SFGs, and a lower normalization, i.e.,

¹ University of California, Santa Cruz

² University of California, Berkeley

³ The Hebrew University

⁴ Pennsylvania State University

⁵ Hubble Fellow

⁶ Universidad Complutense de Madrid

⁷ Space Telescope Science Institute

⁸ Santa Cruz Institute for Particle Physics

⁹ Rutgers University

¹⁰ University of Missouri

¹¹ Shenyang Normal University

¹² Centro de Astrobiología, CSIC-INTA

¹³ Colby College

higher densities (Williams et al. 2010; Newman et al. 2012; van der Wel et al. 2014). While both the SFR-MS and the size-mass scaling relations evolve with time, the fundamental structural differences in SFGs and quiescent galaxies are always present, suggesting that having concentrated (denser) surface density profiles is a requisite for quenching (Kauffmann et al. 2003, 2006; Schiminovich et al. 2007; Bell 2008; Cheung et al. 2012; Fang et al. 2013; Lang et al. 2014). In other words, SFGs must grow dense stellar cores before quenching.

There is increasing observational evidence that SFGs with dense cores exist at every redshift. At $z \gtrsim 2$, SFGs with the highest central densities are remarkably compact and have high Sérsic indices and spheroidal morphologies, lacking any signature of an underlying disk (Wuyts et al. 2011b; Barro et al. 2013, 2014a,b; Patel et al. 2013; Stefanon et al. 2013; Williams et al. 2013; Nelson et al. 2014). These galaxies resemble the quiescent population at the same redshift but are radically different from other SFGs that have irregular and clumpy appearances (Elmegreen et al. 2004; Genzel et al. 2008; Guo et al. 2015). This suggests that compact SFGs are formed by strongly dissipational processes. Some of these processes, like mergers and disk instabilities, are indeed expected to be more frequent at earlier times due to the higher gas-to-total mass ratios in SFGs (Tacconi et al. 2010, 2013; Daddi et al. 2010). The increased gas mass relative to the SFR makes such systems prone to gravitational collapse on scales of ~ 1 kpc, causing substantial core-growth resulting from a gas-fed central starburst and/or an inward migration of clumps (Dekel et al. 2009b; Ceverino et al. 2010; Genel et al. 2014; Wellons et al. 2014; Ceverino et al. 2015; Zolotov et al. 2015). At lower redshifts, SFGs with dense stellar cores have clearly recognizable disk structures, but their profiles are dominated by a central bulge (Wuyts et al. 2012; Bruce et al. 2012; Bruce et al. 2014a; Lang et al. 2014). Interestingly, quiescent galaxies at low- z also seem to have bulge+disk morphologies (McGrath et al. 2008; Bundy et al. 2010; van der Wel et al. 2011), suggesting that quenching takes place among galaxies with similar morphologies.

The common denominator in the evolution of massive galaxies described above is the growth of a dense stellar core. This suggests that it is possible to describe the general processes of structural growth and star-formation quenching using a unique quantity tracing central stellar mass density. Here we study the evolution since $z \sim 3$ of the stellar mass surface density within a radius of 1 kpc, Σ_1 . We build upon previous results at lower redshift which show that Σ_1 is closely related with quiescence, and follows a much tighter correlation with stellar mass than the effective radius or the effective surface density, Σ_e (e.g., Cheung et al. 2012, Fang et al. 2013; van Dokkum et al. 2014; Woo et al. 2015). We aim to answer whether this relation holds at high redshift, if it is a more fundamental quenching predictor, and if the global build up and quenching of SFGs can be described in simple terms using Σ_1 , i.e., if it can be used to track galaxies in transit from the star-forming to quiescence phase.

The paper is structured in three parts: In § 2, we give an overview of the observational dataset and the esti-

mated properties of the galaxy sample. In § 3.1 we analyze the correlations in effective and central mass surface densities, Σ_e and Σ_1 , vs. stellar mass for SFGs and quiescent galaxies from $z = 3 - 0.5$. In § 3.2 we study how the best-fit relations in Σ_e and Σ_1 relate to each other for galaxies with a Sérsic mass profile. In § 3.4 we analyze galaxy evolutionary paths based on the best-fit $\Sigma_{e,1}$ structural relations and predictions of hydrodynamical simulations. We find that the structural evolution of SFGs can be described in terms of 2 phases: A steady phase of size and core growth that we call the Σ “main sequence”, and a “compaction” phase of rapid core growth. In § 3.5 we study the relative distance of massive SFGs and quiescent galaxies from the SFR-MS and the quiescent structural relations as a function of redshift. We find that their distribution defines a universal (redshift-independent) L-shape sequence that traces 2 fundamental transformations: the compaction of SFGs to form a dense stellar core, and the quenching of star-formation in those galaxies at maximum central density. Lastly, in § 3.6 we discuss the evolution in the structural properties and visual morphologies of galaxies within the compaction-quenching sequence as a function of time.

Throughout this paper, we quote magnitudes in the AB system, assume a (Chabrier 2003) initial mass function (IMF) and adopt the following cosmological parameters: $(\Omega_M, \Omega_\Lambda, h) = (0.3, 0.7, 0.7)$.

2. DATA

This paper is based on a sample of massive galaxies built from the *HST*/WFC3 F160W selected catalog for the CANDELS GOODS-S field (Guo et al. 2013). Consistent, multi-wavelength photometry was measured using TFIT (Laidler et al. 2006), implemented as described by Guo et al. (2012). Photometric redshifts were computed using EAZY (Brammer et al. 2008) and yielded errors of $\Delta z/(1+z) = 3\%$. Stellar masses were derived using FAST (Kriek et al. 2009b) and based on a grid of Bruzual & Charlot (2003) models that assume a Chabrier (2003) IMF, solar metallicity, exponentially declining star formation histories, and the Calzetti et al. (2000) dust extinction law (see Santini et al. 2015 for a detailed description).

Star formation rates (SFRs) were computed by combining IR and rest-frame UV (uncorrected for extinction) luminosities (Kennicutt 1998 and Bell et al. 2005) and adopting a Chabrier (2003) IMF (see Barro et al. 2011 for more details): $SFR_{UV+IR} = 1.09 \times 10^{-10} (L_{IR} + 3.3L_{2800})$. Total IR luminosities ($L_{IR} \equiv L[8-1000\mu\text{m}]$) were derived from Chary & Elbaz (2001) templates fitting MIPS $24\mu\text{m}$ fluxes, applying a *Herschel*-based recalibration (Elbaz et al. 2011). For galaxies undetected by MIPS below a 2σ level ($20\mu\text{Jy}$) SFRs come from rest-frame UV luminosities that are corrected for extinction as derived from SED fits (Wuyts et al. 2011a).

The half-light radii, measured along the major axis, and Sérsic indices were determined from *HST*/WFC3 *H* images using GALFIT (Peng et al. 2002) with PSFs created and processed to replicate the conditions of the observed data (van der Wel et al. 2012). The stellar mass profiles were computed by fitting multi-band SEDs derived from surface brightness profiles in 9 HST bands measured with IRAF/ellipse (see Liu et al. 2013 and Liu et al. in prep for more details). Following Wuyts et al.

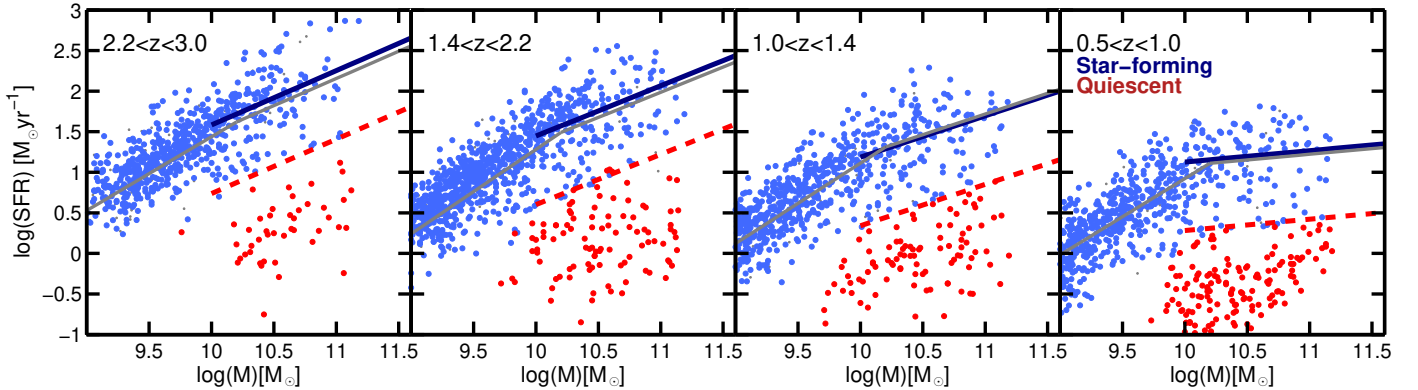


FIG. 1.— Star-formation rate vs. stellar mass for galaxies in the CANDELS/GOODS-S field at $0.5 < z < 3.0$. The blue lines show our fits to the SFR-MS at each redshift, which agree with previous results above $\log(M/M_\odot) > 10$. The gray lines show the results of Whitaker et al. (2013), which highlight the change in the slope of the SFR-MS at lower masses. SFGs are indicated by the blue points. Quiescent galaxies (red points) are selected to lie 0.7 dex below the SFR-MS, i.e., below the red dashed lines.

(2012), we impose an additional constraint on the spatially resolved SED-fit by requiring that the integrated profile matches the observed flux in IRAC ch1 and ch2. We apply this constraint by assuming that the integrated IRAC-F160W color is the same at all radii.

The multi-band HST mosaics were PSF-matched to the resolution of F160W, that has a half width at half maximum of $\text{HWHM}=0.''09$. The profiles have an intrinsic spatial resolution ranging from $r = 0.6 - 0.7$ kpc within the redshift range of the sample and thus resolve the inner 1 kpc of the galaxies. However, part of the light can be smeared to larger radius. To correct for this effect, we estimate a Sérsic dependent correction to the mass profile within 1 kpc. The correction is computed from a grid Sérsic profiles with $n = 0 - 4$ and $r_e = 0.1 - 10$ kpc degraded to F160W resolution at different redshift. The correction ranges from ~ 0.4 dex at $n \gtrsim 2$ to $\sim 0.2 - 0$ dex at $n = 1 - 0$.

Our goal is to analyze the distribution of massive SFGs and quiescent galaxies at $0.5 < z < 3$ in the structural scaling relations in order to understand their differential evolution. The deep CANDELS photometry enables the selection of stellar mass complete samples down to $\log(M/M_\odot) \sim 10.3$ at $z = 3$ (e.g., Tal et al. 2014). Thus, we use this threshold to limit our sample selection for the analysis in § 3.4 and 3.5. Nonetheless, in the next section, we use a larger sample of galaxies down to $\log(M/M_\odot) = 9$ ($\sim 70\%$ complete) to characterize the SFR and structural correlations over a wider dynamical range.

3. RESULTS

3.1. SFR and structural scaling relations

Figure 1 show the distribution of SFR vs. stellar mass for the galaxies in GOODS-S. The majority of star-forming galaxies follow a relatively tight relation between SFR and stellar mass. The observed relation suggests that galaxy star formation histories are predominantly regular and smooth, i.e., galaxies grow in a secular mode which is usually referred to as the SFR main sequence (SFR-MS; Noeske et al. 2007; Elbaz et al. 2007; Salim et al. 2007; Pannella et al. 2009; Magdis et al. 2010; Wuyts et al. 2011a; Elbaz et al. 2011; Rodighiero et al. 2010; Whitaker et al. 2012;

Pannella et al. 2014). Following previous works, we characterize the SFR-MS as a single power-law at $\log(M/M_\odot) \gtrsim 10$.

$$\log \text{SFR} = \mu \left[\log \left(\frac{M_\star}{M_\odot} \right) - 10.5 \right] + \log C \quad (1)$$

Note that at lower masses, the SFR-MS exhibits a steeper slope (e.g., Whitaker et al. (2014); Schreiber et al. (2015)). The best-fit SFR-MS at every redshift is in excellent agreement with the results of Whitaker et al. (2014) and Schreiber et al. (2015) at the high-mass end. The slope and the normalization are consistent with their values within the errors (Table 1). We select star-forming galaxies above and quiescent galaxies below a threshold of $\Delta \text{SFR} = -0.7$ dex (dashed red line), where $\Delta \text{SFR} \equiv \log \text{SFR} - \log \text{SFR}^{\text{MS}}$. This classification line is $\sim 2\sigma$ below the SFR-MS, which has a typical observational scatter of 0.3 dex (Whitaker et al. 2014; Speagle et al. 2014; Schreiber et al. 2015).

Panel A of Figure 2 shows the distribution in effective surface mass density, $\Sigma_e = 0.5M_\star/\pi r_e^2$, vs. mass for the galaxies in Figure 1. SFGs and quiescent galaxies follow well-defined size-mass relations, which are characterized by low-linear relations, $\log r_e \propto a \log M$ (e.g., Law et al. 2012; Mosleh et al. 2012; Szomoru et al. 2012; Newman et al. 2012; van der Wel et al. 2014). Those relations can be expressed in terms of Σ_e :

$$\log \Sigma_e = \alpha \left[\log \left(\frac{M_\star}{M_\odot} \right) - 10.5 \right] + \log A(z) \quad (2)$$

where α is related to the slope of the size-mass relation a as $\alpha = 1 - 2a$. The red and blue lines show the best-fit Σ_e relations for quiescent and star-forming galaxies. The best-fit slopes are relatively constant with time, $\alpha^{\text{SF}} \sim -0.5$, $\alpha^{\text{Q}} \sim 0.6$ and agree well with the results of van der Wel et al. (2014) for the size-mass relations of both populations ($a^{\text{SF}} \sim 0.2$ and $a^{\text{Q}} \sim 0.8$). There are too few quiescent galaxies at $2.2 < z < 3.0$ to accurately fit the slope, and so we fix the slope (but not the normalization) in this bin to match the value at $1.4 < z < 2.2$. Note that quiescent galaxies have a steep slope in the size-mass relation, which leads to an anti-correlation in Σ_e^{Q} . Meanwhile, SFGs have a shallow slope

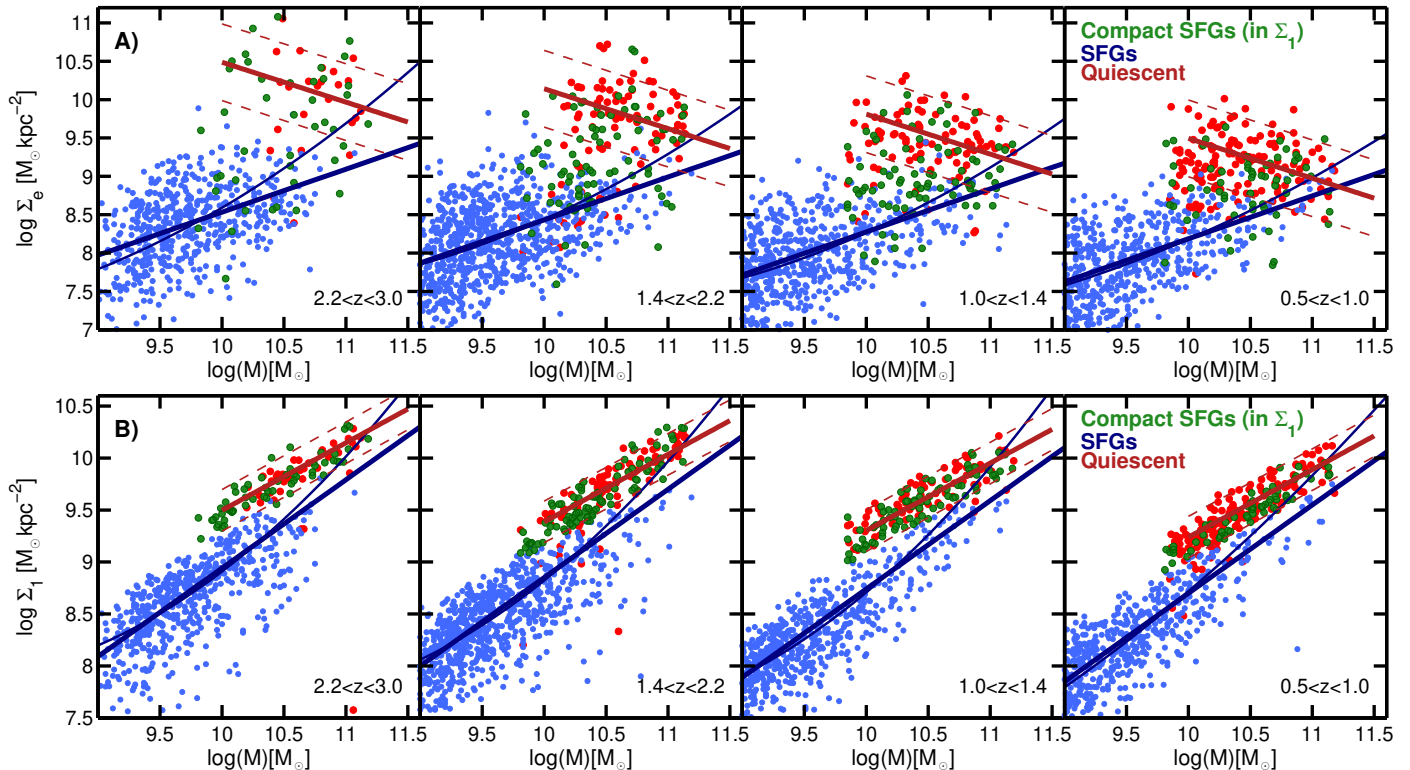


FIG. 2.— Surface density vs. stellar mass for galaxies in the CANDELS/GOODS-S field at $0.5 < z < 3.0$. Panels A and B show the surface density within the effective radius, Σ_e , and within the inner 1 kpc, Σ_1 , respectively. The blue and red circles show SFGs and quiescent galaxies selected using the SFR criterion of Figure 1. The thick blue and red lines depict the best-fit $\log \Sigma - \log M_*$ relations for the two populations. The dashed red lines show the 2σ scatter around the quiescent relation. SFGs and quiescent galaxies exhibit clear and distinct scaling relations since $z \sim 3$, which are well-described by single power-laws. The scatter in the Σ_1 relations is a factor of ~ 2 smaller than that of Σ_e . The slopes of the scaling relations remains approximately constant with time. The zero-points of the star-forming relations decline slowly with time (see Figure 3). Based on this smooth evolution, we speculate that SFGs follow, on average, evolutionary paths along that relation. We define this track as a structural “main sequence” (Σ -MS). At $\log(M/M_\odot) \gtrsim 10$ we find an increasing number of compact SFGs with high surface densities, similar to those of quiescent galaxies (green circles selected within Σ_1). We capture this trend by fitting a second-order polynomial to $\log \Sigma - \log M_*$, which shows a steeper slope at the high-mass end (thin blue line). These galaxies may deviate upwards from the Σ -MS due to dissipational “compaction” events that cause a rapid core growth (see § 3.4.2). Fit parameters are given in Tables 1 and 2

in size-mass ($a^{\text{SF}} < 0.5$) and a positive correlation between Σ_e^{SF} and mass. The scatter in Σ_e is consistent with $\sim 2\times$ that of the size-mass relations, $\sigma(\log \Sigma_e) \sim 0.5$ dex and 0.3 dex, for SFGs and quiescent galaxies, as expected from $\Delta \log \Sigma_e \propto 2\Delta \log r_e$. The redshift-dependent normalizations decline from $z = 3$ to $z = 0.5$. Such decline is much steeper for quiescent galaxies than for SFGs (1 dex vs. 0.3 dex) as noted in previous works (Buitrago et al. 2008; Newman et al. 2012; van der Wel et al. 2014).

The bottom row (B panels) of Figure 2 shows the redshift evolution of the central surface mass density within 1 kpc, $\Sigma_{1\text{kpc}} = M(< 1 \text{ kpc})/\pi(1 \text{ kpc})^2$, versus the stellar mass. Similarly to Σ_e , we characterize the observed correlation in Σ_1 as a log-linear relation:

$$\log \Sigma_1 = \beta \left[\log \left(\frac{M_*}{M_\odot} \right) - 10.5 \right] + \log B(z) \quad (3)$$

Again, we find clear correlations for both SFGs and quiescent galaxies at every redshift since $z \sim 3$. The slopes of these relations are positive and relatively constant with time, $\beta^{\text{SF}} = 0.9$ and $\beta^{\text{Q}} = 0.7$. By comparison with Σ_e , the dispersion is $\sim 2\times$ tighter, $\sigma(\log \Sigma_1) \sim 0.25$ dex and 0.14 dex, for SFGs and quiescent galaxies, in good agreement with the results of Fang et al. (2013) at $z = 0$. The normalization of the star-forming Σ_1^{SF} relation de-

clines by ~ 0.3 dex from $z = 3$ to $z = 0.5$ similar to the evolution in Σ_e^{SF} . Interestingly, for quiescent galaxies, Σ_1^{Q} declines by a similar amount, in stark contrast with the strong decline of ~ 1 dex in Σ_e^{Q} . The lower scatter and weaker redshift evolution indicates that Σ_1 is a more robust and reliable structural parameter than Σ_e . Note also that, by measuring the mass inside a fixed physical core aperture, Σ_1 is closer to the concept of a cosmic *clock*, i.e., it only increases with a stellar mass growth, unlike the effective size (r_e), which can also decrease (e.g., due to a substantial mass growth closer to galaxy center, or to fading of an extended star-forming region).

Two main conclusions arise from the distribution of SFGs and quiescent galaxies in Figure 2: 1) the slopes of the structural relations are almost constant with time, and the normalizations decline for all of them; 2) at any redshift, quiescent galaxies are denser than SFGs of the same mass, although this difference declines with time in Σ_e due to fast evolution of Σ_e^{Q} . A reasonable assumption based on the first conclusion is that the evolutionary paths of individual SFGs approximately follow the best-fit Σ_e^{SF} relation which, by analogy with the SFR-MS, defines a structural main sequence, Σ -MS, that could be interpreted as phase of smooth structural growth. The

TABLE 1
POWER LAW FITS

redshift range	$SFR_{MS} - \text{SFGs}$		$\Sigma_e - \text{Quiescent}$		$\Sigma_e - \text{SFGs}$		$\Sigma_1 - \text{Quiescent}$		$\Sigma_1 - \text{SFGs}$	
	μ	$\log C$	α	$\log A$	α	$\log A$	β	$\log B$	β	$\log B$
$0.5 < z < 1.0$	0.19 ± 0.08	1.21 ± 0.02	-0.42 ± 0.13	9.15 ± 0.06	0.60 ± 0.04	8.46 ± 0.04	0.65 ± 0.03	9.53 ± 0.05	0.89 ± 0.03	9.12 ± 0.03
$1.0 < z < 1.4$	0.53 ± 0.07	1.44 ± 0.04	-0.45 ± 0.14	9.53 ± 0.05	0.60 ± 0.05	8.54 ± 0.05	0.65 ± 0.04	9.64 ± 0.04	0.88 ± 0.03	9.16 ± 0.04
$1.4 < z < 2.2$	0.64 ± 0.06	1.75 ± 0.05	-0.52 ± 0.14	9.91 ± 0.07	0.64 ± 0.05	8.68 ± 0.04	0.64 ± 0.03	9.74 ± 0.05	0.86 ± 0.04	9.25 ± 0.03
$2.2 < z < 3.0$	0.68 ± 0.06	1.92 ± 0.05	-0.48 ± 0.17	10.16 ± 0.05	0.56 ± 0.06	8.80 ± 0.04	0.67 ± 0.04	9.80 ± 0.05	0.89 ± 0.04	9.33 ± 0.05

Notes. power law coefficients parameterizing the evolution of the SFR ($\log \text{SFR} = \mu \log(M_\star - 10.5) + \log C$), the effective mass surface density ($\log \Sigma_e = \alpha \log(M_\star - 10.5) + \log A$) and the mass surface density within the central 1 kpc ($\log \Sigma_1 = \beta \log(M_\star - 10.5) + \log B$) relations with stellar mass as a function of redshift.

TABLE 2
2ND-ORDER POWER LAW FITS

redshift range	$\Sigma_e - \text{SFGs}$			$\Sigma_1 - \text{SFGs}$		
	α_1	α_2	$\log A$	β_1	β_2	$\log B$
$0.5 < z < 1.0$	0.09 ± 0.08	1.10 ± 0.07	9.25 ± 0.03	0.08 ± 0.04	0.80 ± 0.03	8.56 ± 0.05
$1.0 < z < 1.4$	0.15 ± 0.07	1.19 ± 0.06	9.25 ± 0.02	0.08 ± 0.03	0.95 ± 0.04	8.65 ± 0.04
$1.4 < z < 2.2$	0.16 ± 0.06	1.18 ± 0.07	9.36 ± 0.02	0.09 ± 0.03	1.12 ± 0.03	8.82 ± 0.05
$2.2 < z < 3.0$	0.14 ± 0.06	1.10 ± 0.05	9.41 ± 0.02	0.11 ± 0.04	1.10 ± 0.04	8.93 ± 0.05

Notes. Power law coefficients parameterizing the evolution of Σ_e and Σ_1 vs. stellar mass as 2nd order polynomials: $\log \Sigma_e = \alpha_1 (\log M)^2 + \alpha_2 \log M + \log A$ and $\log \Sigma_1 = \beta_1 (\log M)^2 + \beta_2 \log M + \log B$

second conclusion indicates that increasing the surface density by forming a dense stellar core is a requisite for quenching the star-formation, as similarly suggested in previous works. Together, these conclusions suggest the need for an intermediate phase to bridge the Σ -MS and quiescent sequence, in which SFGs become more compact and centrally concentrated before quenching. We further discuss the possible evolutionary paths of SFGs and quiescent galaxies in § 3.4.

3.2. Surface mass profiles: relating Σ_e and Σ_1

In this section we analyze the relation between the Σ_e and Σ_1 structural relations for SFGs and quiescent galaxies in terms of their surface density profiles. Galaxies's surface brightness and stellar mass profiles are typically described by Sérsic (1963) profiles, in which case, the central and effective densities are related to one another by the profile parameters. Assuming the following characterization of the mass profile:

$$M(r) = M_e \exp\left(-b_n \left[\left(r/r_e\right)^{1/n} - 1\right]\right) \quad (4)$$

where n is the sersic index and M_e is the effective mass at r_e , Σ_1 and Σ_e can be determined from one of them for a given value of n and r_e . Note that in doing so we assume that the mass and light profiles are the same, $r_{e,\text{mass}} = r_{e,\text{light}}$. This is a better approximation for quiescent galaxies, which exhibit only weak color gradients (e.g., Guo et al. 2012; Szomoru et al. 2012; Wuyts et al. 2012). Nonetheless, the parametrization is useful to discuss the expected differences in Σ_1 and Σ_e when the assumption fails.

By integrating Equation 4 we obtain:

$$\log \Sigma_{1\text{kpc}} - \log M_\star = -\log \pi - \log \gamma(2n, b_n r_e^{-1/n}) \quad (5)$$

where γ is the incomplete gamma function, which depends on n and r_e (see e.g., Graham et al. 2005). As

shown in Figure 4, the γ function can be approximated as a second order polynomial for a given n .

$$\log \gamma(2n, b_n r_e^{-1/n}) = c_0 + c_1 \log r_e + c_2 (\log r_e)^2 \quad (6)$$

where the c_i coefficients depend on the Sérsic index. Combining the linear term of this equation with the best-fit relations for Σ_1 and Σ_e as a function of mass, and the definition of the latter in terms of r_e ($\log r_e = 0.5(\log M_\star - \log \Sigma_e)$), we obtain the following relations for the slope and the scatter of the $\log \Sigma_1 - \log M_\star$ relation in terms of the slope in the Σ_e and size-mass relations.

$$\begin{aligned} \beta &\sim 1 + 0.5c_1(\alpha - 1); & \sigma(\log \Sigma_1) &\sim 0.5c_1\sigma(\log \Sigma_e) \quad (7) \\ \beta &\sim 1 - c_1a; & \sigma(\log \Sigma_1) &\sim c_1\sigma(\log r_e) \end{aligned}$$

Quiescent galaxies typically have high Sérsic values, $n = 3 - 4$ (Williams et al. 2010; Bell et al. 2012). Therefore, for a value of $c_1(4) = 0.55$, we obtain $\sigma(\log \Sigma_1) \sim 0.3\sigma(\log \Sigma_e)$, which explains the smaller scatter in Σ_1 with respect to Σ_e . Furthermore, for a value of $\alpha \sim -0.5$, the expected slope of the Σ_1^Q relation is $\beta \sim 0.6$, which is consistent with the best-fit value. Thus, a single Sérsic model is good approximation to explain the differences in the Σ_1^Q and Σ_e^Q relations.

SFGs exhibit a broad range in Sérsic values, and their profiles can often deviate from a single Sérsic profile, e.g., in a disk with a denser bulge (Wuyts et al. 2011a; Bruce et al. 2012). The color code in Figure 5 illustrates the spread in Sérsic values for SFGs in the Σ_1 vs. mass diagram. At a given stellar mass, the Sérsic increases with Σ_1 . This correlation suggest that as SFGs grow a dense stellar core, their mass profiles become more centrally concentrated. I.e., the width of the Σ_1 distribution for SFGs depends on their structural properties. The SFGs in the overlapping region with Σ_1^Q , in particular, exhibit Sérsic values similar to those of quiescent galaxies. The blue and cyan lines show the predicted Σ_1^{SFG} relation based on Σ_e^{SFG} for $n = 1$ and $n = 2$. Qualitatively, the predic-

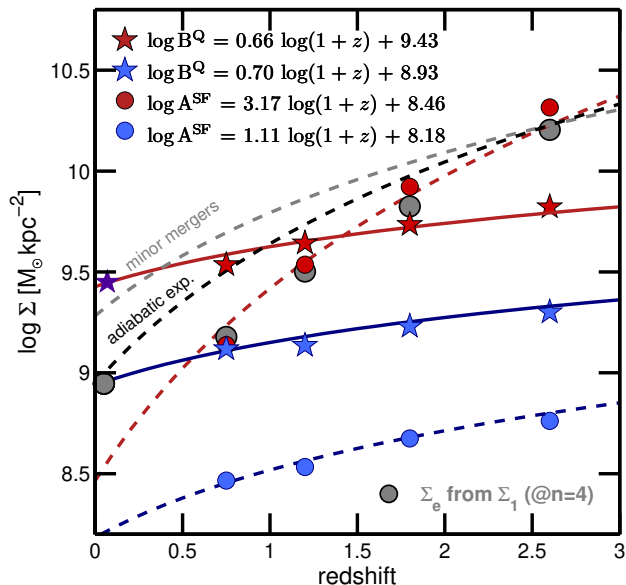


FIG. 3.— Redshift evolution in the normalization of the Σ_1 (stars; log B) and Σ_e (circles; log A) relations for SFGs (blue) and quiescent galaxies (red). The solid and dashed lines show the best-fit relations to the normalizations in Σ_1 and Σ_e as a function of redshift. The purple star shows the zero-point of the quiescent Σ_1 relation at $z = 0$ from Fang et al. (2013). The dashed gray line shows the predicted evolution in Σ_e^Q due to minor mergers, assuming that Σ_1^Q evolves only due to mass growth outside 1 kpc. The dashed black line shows the predicted evolution in Σ_e^Q assuming that Σ_1^Q evolves only due to mass loss and adiabatic expansion. The gray circles show the predicted normalization in Σ_e^Q inferred from Σ_1^Q using Equation 5 and a Sérsic of $n = 4$.

tion for $n = 2$ matches the slope and normalization of the best-fit Σ_1^{SFG} relation (gray). However, the relations determined from Σ_e^{SFG} with $n \lesssim 2$ have lower normalizations than the observed distribution of SFGs with similar Sérsic values. This suggests that the normalization of the Σ_e distribution for SFGs also increases with n .

3.3. Redshift evolution of the normalization of the quiescent structural relations

Using equation 5 and the relation between Σ_e and r_e , we quantify the evolution in the normalization of the structural relations (log A and log B) due to different evolutionary processes that preserve the Sérsic profile but cause a relative change in size and stellar mass characterized as $\Delta \log r_e = \eta \Delta \log M$. If the slope of the structural relations remain constant in the process, the normalizations change as $\Delta \log \Sigma_{e,1} - (\alpha, \beta) \Delta \log M$, which leads to:

$$\begin{aligned} \Delta \log A &= (1 - 2\eta - \alpha) \Delta \log M \\ \Delta \log B &\sim (1 - c_1 \eta - \beta) \Delta \log M \end{aligned} \quad (8)$$

These relations are useful to test whether some of the proposed evolutionary processes are consistent with the simultaneous evolution in the normalizations of both structural relations (Table 1). For quiescent galaxies, where the relative evolution in the normalization of Σ_e vs. Σ_1 is largest, there are three main evolutionary channels that can explain such large difference. The leading explanation is that quiescent galaxies experience a large increase in size compared to the mass

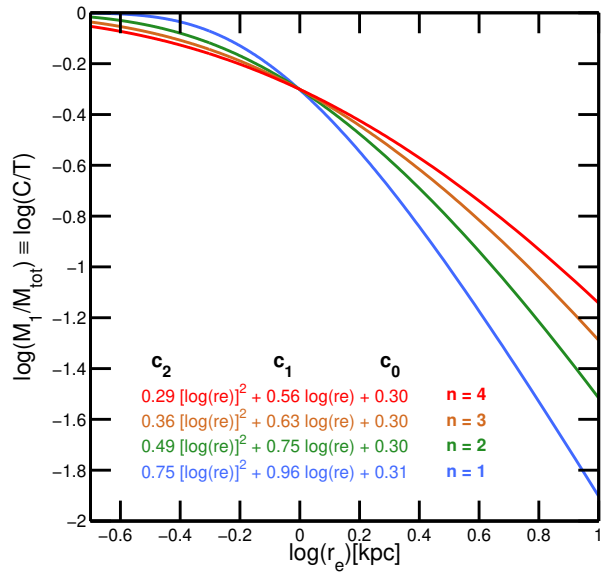


FIG. 4.— Ratio of the mass in the central 1 kpc to the total mass (defined as C/T) as a function of the effective radius, r_e , and n for a single-Sérsic mass profile. The C/T ratio follows a gamma function (Equation 5), which can be expressed as a second-order polynomial in r_e for different values of n (bottom-left corner; Equation 6). The linear coefficient of those relations, c_1 , determines the relative values of the slope and typical scatter of the Σ_e , Σ_1 and r_e scaling relations with stellar mass (Equation 7). The best-fit structural relations for quiescent galaxies, Σ_e^Q and Σ_1^Q agree well with one another for a Sérsic profile of $n = 4$ (see gray and red lines in Figure 5).

growth due to minor mergers (i.e., accretion of smaller satellite galaxies; Bezanson et al. 2009; Hopkins et al. 2009; Oser et al. 2012). Alternatively quiescent galaxies can have a large increase in size (*puff up*) due to feedback or stellar mass loss associated with passive evolution (i.e., death of old stars) which cause adiabatic expansion (Damjanov et al. 2011; Poggianti et al. 2013; Porter et al. 2014; van Dokkum et al. 2014). Lastly, the strong decline in Σ_e^Q could be caused by the arrival of new quiescent with progressively larger sizes at lower redshifts (e.g., Poggianti et al. 2013; Carollo et al. 2013; Porter et al. 2014). Each of these scenarios leads to a different evolution in the normalization of Σ_e^Q and Σ_1^Q . Attending to the best-fit relations in the upper-left corner of Figure 3, the expected evolution in the ratio of normalizations is $\Delta \log A / \Delta \log B \sim 5$.

If the evolution of quiescent galaxies is driven by minor mergers, the expectation is that the core mass remains relatively unchanged in the process. Thus the normalization in Σ_1^Q changes only due to the total mass growth as $\Delta \log B \sim -0.65 \Delta \log M$, while the normalization in Σ_e^Q follows Equation 8 as $\Delta \log A \sim -1.7 \Delta \log M$, for conservative value of $\eta \sim 1.6$ (e.g., Newman et al. 2012). The predicted relative change in such case is $\Delta \log A / \Delta \log B \sim 2.6$, which is substantially lower than the observed ratio (gray line in Figure 3). Therefore a simple minor merger scenario is inconsistent with the observed results. This tension can be partially alleviated if mergers cause a larger size growth ($\eta \gg 1.6$) or if they also cause an increase in Σ_1 , e.g., due to projection effects in the 2D surface density. The latter, however, is inconsistent with the results of van Dokkum et al. (2014),

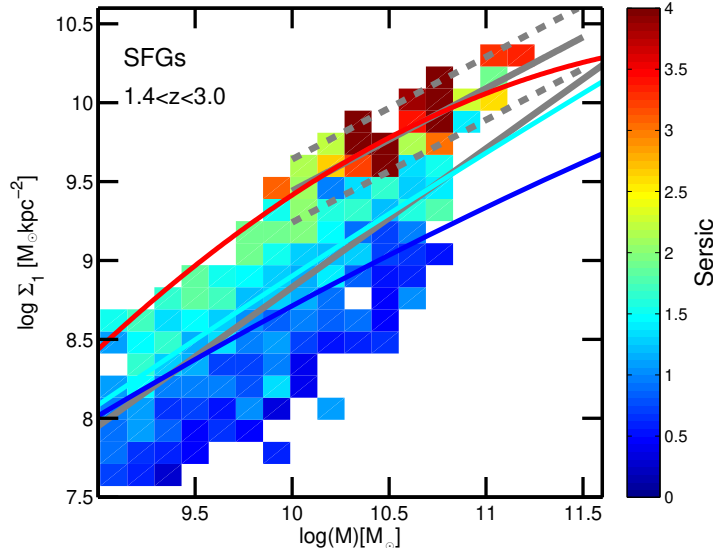


FIG. 5.— Σ_1 vs. stellar mass for only SFGs at $1.4 < z < 3.0$ color coded by median Sérsic index. The gray lines show the best-fit $\log \Sigma_1 - \log M_*$ relations for SFGs and quiescent galaxies at $z = 2$ depicted in Figure 2. The SFGs in the overlapping region with the quiescent Σ_1 relation (dashed gray lines) exhibit higher Sérsic index. This could indicate that those SFGs arrive on the quiescent sequence as a result of a structural transformation that makes their mass profiles more centrally concentrated. The red line shows the Σ_1^Q relation inferred from the observed Σ_e^Q relation for quiescent galaxies using Equations 5 and 6 and Sérsic value of $n = 4$. The observed and predicted Σ_1 relations show an excellent agreement. The blue and cyan lines show the predicted Σ_1^{SF} relation for SFGs derived from Σ_e^{SF} assuming $n = 1$ and $n = 2$, respectively. Qualitatively, the slopes agree with the observed relation, but the systematically lower normalizations suggest that the zero-point of Σ_e^{SF} depends on the Sérsic.

who showed that the number density of the most massive cores decreases with time.

An alternative, or most likely complementary, scenario to explain the fast decline in the normalization of Σ_e^Q is that newly quenched galaxies at lower redshifts have larger sizes and lower density cores (e.g., Poggianti et al. 2013; Carollo et al. 2013). Assuming that all those quiescent galaxies have also high Sérsic indices ($n \sim 4$), we use equations 5 and 6 estimate the redshift dependent normalization in Σ_e^Q based on the observed values of the the normalization in Σ_1^Q (gray circles in Figure 3). This prediction exhibits a much better agreement with observations down to $z = 0.75$, suggesting that a single Sérsic model is a good approximation at those redshifts. The main difference with a minor merger scenario is that the latter increases the size and preserves the core density at the expense of breaking the single Sérsic mass profile. Note however that at $z = 0$, the predicted value of Σ_e^Q based on the Σ_1^Q value of (Fang et al. 2013) deviates from the expected trend towards larger sizes for a given central density. This could signal a more prominent role of minor mergers at lower redshifts or a change in the ratio of wet-to-dry mergers (e.g, López-Sanjuan et al. 2012; Porter et al. 2014).

Another evolutionary scenario that preserves the shape (Sérsic index) of the mass profile is adiabatic expansion. In this case, galaxies puff up due to a decline in the gravitational potential caused by the death old stars.

For a value of $\eta = -1$ (e.g., Damjanov et al. 2009), Σ_e^Q decreases as $\Delta \log A \sim 3.5 \Delta \log M_*$, while Σ_1^Q decreases as $\Delta \log B \sim \Delta \log M_*$. Thus, the ratio between the two is $\Delta \log A / \Delta \log B \sim 3.5$, which is larger than the prediction from minor mergers, but still underestimates the observed trend (dashed black line). The nearly unity relation in $\log B$ with stellar mass indicates that the mass loss required to reproduce the observed evolution in Σ_1^Q from adiabatic expansion is $\Delta \log M_* \sim (1+z)^{0.66}$ (Figure 3). However, as noted by van Dokkum et al. (2014), a simple formation model in which quiescent galaxies quenched as early as $z \sim 5$ implies a much slower mass decline ($\sim (1+z)^{0.06}$).

As pointed out in previous works, the most likely scenario is that all the evolutionary channels above play a role in the evolution of the normalizations. Nonetheless, quantifying their relative contribution as a function of time requires precise estimates of the ages and quenching times of quiescent galaxies (e.g., Belli et al. 2014b), as well as large enough samples to characterize the number densities at the extremes of the distributions (i.e., the smallest or densest galaxies) whose disappearance indicates the need for a size growth van der Wel et al. 2014) or mass loss (van Dokkum et al. 2014).

In passing, we note that the decreasing trend with time in Σ_1 has also implications for the galaxy dynamics. Fang et al. (2013) found an excellent correlation in Σ_1 and the velocity dispersion in the central 1 kpc, which closely followed the virial theorem, $\Sigma_1 \propto \sigma^2$. If this correlation holds at high- z , the decrease in $\Delta \log B(z) \sim 0.3$ dex from $z = 3$ to $z = 0$ implies that the Faber-Jackson (Faber & Jackson 1976) relation at $z \gtrsim 2$ should be 0.15 dex higher than the local value, as suggested in Belli et al. (2014a,b).

3.4. Galaxy evolutionary paths in Σ , Σ_1 vs. M_* : the structural “main sequence” and compaction:

In this section we study possible evolutionary paths for SFGs and quiescent galaxies in Σ_e and Σ_1 vs. mass based on the evolution in the normalization of the structural relations computed in § 3.1 and predictions of theoretical simulations.

3.4.1. Observational trends

Based on the conclusions in § 3.1, we speculate that the relatively constant slope and weak evolution of the normalization in Σ_e^{SF} and Σ_1 suggest that SFGs follow evolutionary paths *along* these sequences, which we define as the Σ -MS. In the following discussion we adopt this assumption, and thus we refer to the Σ -MS as log-linear tracks in $\Delta \log \Sigma_{(e,1)} = (\alpha, \beta) \Delta \log M$ with slopes of $\alpha \sim 0.7$ and $\beta \sim 0.9$.

SFGs in the Σ -MS increase their surface density with time. However, since the slope of the Σ_1^{SF} relation is $\beta < 1$ the mass in the core grows more slowly than the total mass of galaxy, i.e., the core-to-total mass ratio decreases with time. This is consistent with the notion of inside-out growth of an exponential profile (disk), due to galactic-scale star-formation and accretion of higher angular momentum material, which causes both r_e and Σ_1 to increase proportionally to the stellar mass growth (e.g., Nelson et al. 2012, 2013). This scenario also agrees with Figure 5, which shows that the Σ -MS (gray) describes an evolution at approximately constant Sérsic.

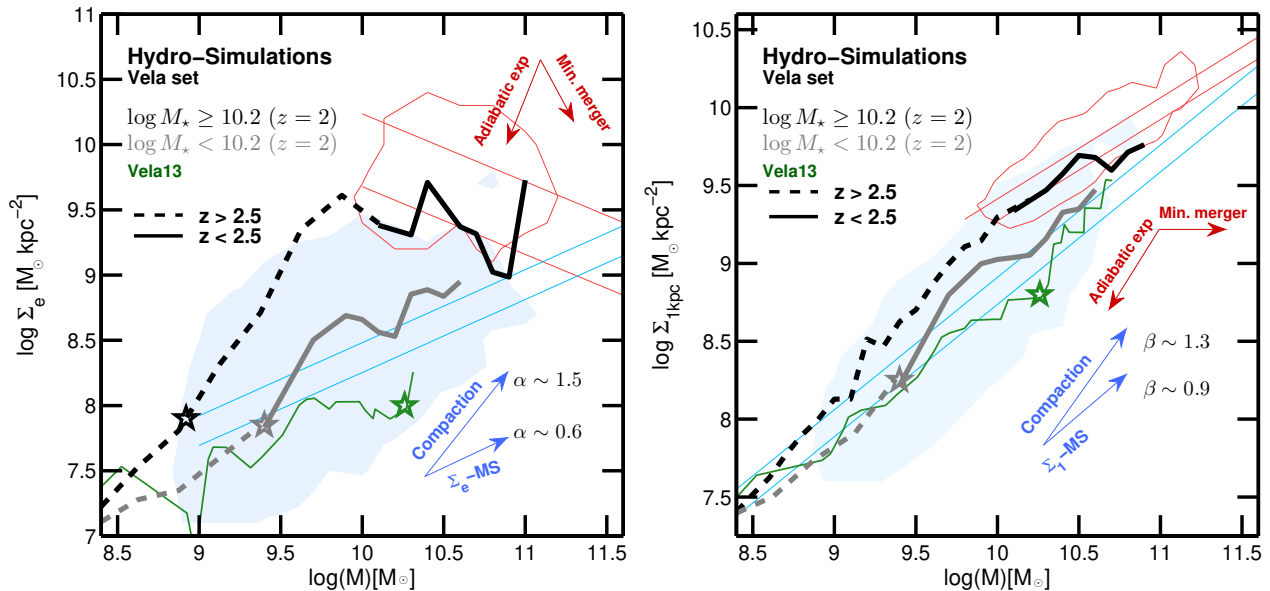


FIG. 6.— Galaxy evolutionary tracks in Σ_e (left) and Σ_1 (right) vs. stellar mass as a function of time for the Vela set of 35 hydrodynamical simulations described in Ceverino et al. (2014) and Zolotov et al. (2015). The black and gray lines show the median evolutionary tracks for galaxies above and below a threshold of $\log(M/M_\odot) = 10.2$ at $z = 2$. The dashed and solid parts of the tracks indicate the evolution at redshift higher and lower than $z = 2.5$, respectively. The blue and red contours show the distribution of SFGs and quiescent galaxies at $z = 1 - 2$. The blue and red lines show the best-fit Σ_e and Σ_1 relations at $z \sim 1$ and $z \sim 2$ from Figure 2. The model tracks are in excellent agreement with the observed distributions in Σ_e and Σ_1 (see also Figure 12 of Ceverino et al. 2015). Moreover, the tracks exhibit two fundamental phases with different slopes (blue arrows): (1) the Σ -MS, a phase of smooth structural growth that follows the best-fit $\Sigma_{e,1}$ relations from the data ($\alpha \sim 0.6$, $\beta \sim 0.9$), and (2) compaction, a period of steep core-growth ($\alpha \sim 1.5$, $\beta \sim 1.3$), usually triggered by a strongly dissipational event (open star) due to higher gas fraction at high- z . The simulations exhibit a *downsizing* trend, such that the most massive galaxies evolve earlier and experience a stronger compaction event (open star) due to higher gas fraction at high- z . The different loci of SFGs and quiescent galaxies is caused by the downsizing trend: massive galaxies form the backbone of the sequence by quenching first (and rapidly) at high- z , while low mass galaxies arrive on the sequence from below in a late compaction event. The green line shows the track of Vela13, which exhibits the latest compaction at $z \sim 1$, remaining the longest in the Σ -MS. The red arrows indicate possible evolutionary tracks for quiescent galaxies for a minor merger or adiabatic expansion scenario (see § 3.3).

For quiescent galaxies, which lack in-situ star-formation, the evolutionary paths are thought to be driven by either minor mergers or adiabatic expansion due to mass loss (see previous section). In a minor merger scenario, quiescent galaxies follow flat tracks in Σ_1 and steeply declining tracks in Σ_e ($\alpha \sim -2.2$). In an adiabatic expansion scenario, quiescent galaxies lose stellar mass and puff up, both within the r_e and the central 1 kpc, which causes a steep decline in Σ_e ($\alpha = -3$) and Σ_1 ($\beta = -1$). The evolutionary tracks for quiescent galaxies in these scenarios are shown as red arrows in Figure 6.

Next, we focus on the evolutionary paths that take SFGs to the higher-density structural relations of quiescent galaxies. To first order, SFGs growing along the Σ -MS intersect the quiescent structural relations at $\log(M/M_\odot) \gtrsim 11.5$. However, confining quenching to this evolutionary track would overproduce the number of massive quiescent galaxies (e.g., van Dokkum et al. 2015). This unique track also requires a population of extremely dense, low mass SFGs that are not observed. An alternative scenario to explain the emergence of quiescent galaxies is that some SFGs follow a steeper path upwards from the Σ -MS as result of some period(s) of fast core growth. These periods can be caused by strongly dissipational, “compaction” events, e.g., major mergers (Hopkins et al. 2008) or disk instabilities (Elmegreen et al. 2008; Dekel et al. 2009b) which funnel large amounts of gas to the center of the galaxy. Compaction events enhance star-formation in the core

increasing the central density and, in the most extreme cases, collapsing the whole galaxy to a much smaller radius.

The compaction scenario was discussed in Wuyts et al. (2011b) and Barro et al. (2013) on the basis that some massive SFGs seem to lie on the steep size-mass relation of quiescent galaxies. These compact SFGs exhibit smaller sizes and higher Sérsic indices than the typical SFGs (see also Figure 5) suggesting that they have experienced a substantial structural transformation. To account for the presence of these compact population on the Σ_e and Σ_1 relations, we fit the $\log \Sigma - \log M_\star$ distribution using a second order polynomial, which allows for a change in the slope at the high mass end. The thin blue lines in Figure 2 indicate that the relations become indeed steeper at $\log(M/M_\odot) \gtrsim 10.5$ in both Σ_e and Σ_1 (see also Table 2) due to the increasing number of SFGs with higher surface densities and Sérsic index (green circles).

In the following, we refer to any evolutionary paths upwards from the Σ -MS due to phase(s) of high-efficiency core growth as compaction track(s). We emphasize that compaction is, primarily, a core building process, and thus it is more efficient at increasing Σ_1 than Σ_e , as the latter depends also on the *overall* galaxy size. See for example the SFGs with dense cores selected within the scatter of Σ_1^Q (green circles in Figure 2) which have a larger scatter in Σ_e . We further discuss this difference in § 3.5.

3.4.2. Trends in hydrodynamical simulations

In order to provide further support for the structural evolutionary paths discussed above, and obtain some insight on the physical mechanism(s) that cause them, we study the evolutionary paths of a sample of high-resolution hydrodynamical simulations in the same parameter space. Figure 6 shows the evolutionary tracks in Σ_1 and Σ_e vs. mass for the Vela set of 35 simulations described in Ceverino et al. (2014) and Zolotov et al. (2015). In the latter, the authors analyzed the SFR, structure and kinematics of the simulated SFGs, showing that the driving force behind the most significant changes in all these properties is a phase (or phases) of dissipational “compaction” caused by, e.g., mergers, disk instabilities, interactions, counter rotating streams or tidal-compressions, which trigger intense episodes of gas inflow and SFR, as mentioned in the previous section.

Following the approach in Zolotov et al. (2015), we divide the sample in two groups according to their mass (in Figure 6, high-mass in black, low-mass in grey), and we show their median evolutionary tracks at early (dashed; $z \geq 2.5$) and late (solid; $z < 2.5$) times. The late evolution matches the redshift range of the galaxy sample, shown as blue and red contours. Qualitatively, the tracks have a similar behavior in both panels, and match the observed distributions. To first order, the overall evolutionary paths can be described in terms of two phases: an early phase of steady structural growth approximately following the slope of the Σ -MS ($\alpha \sim 0.6$, $\beta \sim 0.9$), and a compaction phase, which causes a steep increase in Σ_e and Σ_1 ($\alpha \sim 1.5$, $\beta \sim 1.3$). The steep increase in Σ_e also implies a size shrinkage, particularly in the high-mass simulations (see also Figure 9 in Zolotov et al. 2015). Overall, the dependence on r_e , which can change rapidly due to gas accretion and/or interactions, implies a larger spread in Σ_e with respect to Σ_1 for a given stellar mass.

The main differences in the black and gray tracks are: 1) a *downsizing* effect, i.e., the most massive galaxies evolve earlier and faster; 2) the evolutionary tracks of massive galaxies have a higher normalization; 3) the main compaction event is stronger and happens earlier for the most massive galaxies. The decline in the normalization is the result of a decline in the gas fractions, and thus SFRs, as a function of time (Dekel et al. 2013; Zolotov et al. 2015).

The different loci of SFGs and quiescent galaxies (blue and red contours) also results from the gradual decline in the gas reservoirs and the differential evolution with stellar mass. The quiescent locus consist, almost exclusively, of massive galaxies that experienced a strong compaction event at $z > 2.5$ (black lines in Figure 6). These galaxies quenched star-formation in the core, but continued to grow in stellar mass due to star-formation in a re-grown disk (Zolotov et al. 2015). The new disk causes a sudden increase in size, which leads to decreasing tracks with mass in Σ_e , but nearly flat tracks in Σ_1 . The star-forming locus consist mostly of low mass galaxies which populate the high-mass region at lower redshifts $z < 2.5$ (gray lines). These galaxies experience weaker compaction events, after which the core resumes star-formation and continues on an evolutionary path with a similar slope as the Σ_1 -MS. Later, these SFGs can have a secondary compaction event and arrive on the quiescent sequence from below, as illustrated by the green track of

Vela13. This galaxy has the latest compaction event and thus spends most of its life in the Σ -MS. Interestingly, during the Σ -MS phase, the gas mass in the central 1 kpc remains almost constant, as expected in the case of a simple “bathtub” model evolution (e.g., Dekel et al. 2013). This “bathtub” phase strengthens the notion that the structural main sequence describes a phase of smooth, steady-state evolution that coincides with the SFR main sequence.

Lastly, note that despite the overall agreement in observations and simulations, there are some differences between the simulated tracks and the observed parameter space in Σ vs. mass, particularly at high- z . At $z > 2.5$, all massive SFGs evolve directly into the high-density, quiescent region (red contour) due to strong compaction events, which also cause significant mass growth ($\Delta \log M_\star > 1$ dex). This evolution underpredicts the number of massive SFGs ($\log(M/M_\odot) > 10$) with low Σ_e and Σ_1 at $z > 2.5$, which suggests that the Σ -MS evolutionary channel is underrepresented, or happens only at low redshifts, in this sample simulations.

3.4.3. Summary of evolutionary paths

Based on the excellent agreement in the observed galaxy distributions and model evolutionary tracks in the $\log \Sigma - \log M_\star$ diagrams, we speculate that the overall long-term structural evolution of SFGs can be expressed in terms of 2 fundamental phases, namely, a Σ -MS and compaction. These phases approximately follow linear tracks in $\log \Sigma_{1,e} \propto [\alpha, \beta] \log M_\star$. The Σ main sequence ($\alpha \sim 0.6$, $\beta \sim 0.9$), is a relatively smooth phase of structural growth, consistent with a period of steady-state gas accretion and galactic scale star-formation. As a result, the central and effective densities increase with time, as does the galaxy size, i.e., similar to the typical inside-out growth of a disk. Compaction, is a phase (or phases) of enhanced core-growth ($\alpha > 1$, $\beta > 1$) fueled by strong gas inflow to the galaxy center, as a result of gravitational instabilities. In this phase, the central and effective densities increase steeply, and the galaxy’s effective radius can decrease due to the large increase in stellar mass close to the center or due to a structural collapse. Overall, the intensity and duration of compaction events decreases with time due to the similarly decreasing gas fractions.

For quiescent galaxies, the simulations reproduce the expected evolutionary path of decreasing Σ_e and relatively constant Σ_1 with increasing mass. However, this path is fueled by low levels of in-situ star-formation, which appears to contradict the fast quenching (van de Sande et al. 2013; Bezanson et al. 2013; Onodera et al. 2014) and the lack of diffuse star-forming components (Szomoru et al. 2011, 2012) in quiescent galaxies at $z > 1.5$. The leading theory is that those quiescent galaxies grow due to minor mergers in absence of further star-formation. Alternatively, it could be that some of the SFGs with high surface densities are rejuvenated quiescent galaxies with re-grown star-forming disks. Nonetheless, given the rapidly increasing number of quiescent galaxies (see § 3.5.3) and the lack of apparent disk signatures in those SFGs (see § 3.6), rejuvenated quiescent galaxies with extended star-forming disks can only make a small fraction of the sample.

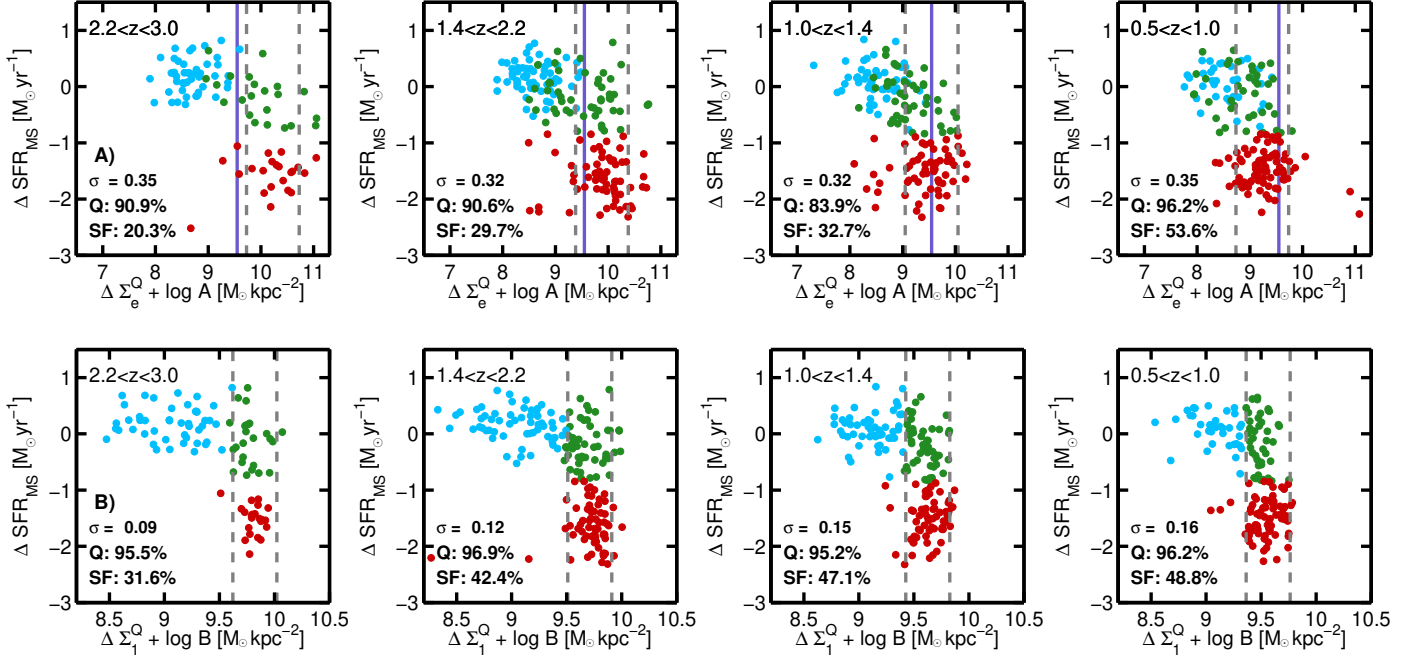


FIG. 7.— ΔSFR vs. $\Delta\Sigma$ plots from the SFR-MS and the Σ_e (top) and Σ_1 (bottom) quiescent structural relations as a function of redshift for galaxies with $\log(M/M_\odot) > 10.3$. The x-axis is normalized to the zero-point of the quiescent relations to illustrate the evolution with time. Blue and green circles indicate SFGs outside and within the 2σ scatter of Σ_1^Q (dashed lines). We refer to the latter as compact SFGs. The relative fractions of SFGs and quiescent galaxies found within the 2σ scatter of Σ_e^Q and Σ_1^Q (dashed lines) are indicated in the bottom left. The L-shaped nature of the distributions indicate that SFGs become compact *before* they quench their star-formation. Moreover, the L-shape persists across redshifts, implying a *universal* process of compaction followed by quenching (see Figure 8). The distributions in the top and bottom panels are very similar; however, Σ_1^Q exhibits a tighter scatter and a much slower evolution of the zero-point. The purple line shows the compactness threshold in Σ_e^Q from B13 which is only efficient at $z \gtrsim 2$. A fraction of the compact SFGs selected with $\Delta\Sigma_1^Q$ are not compact in Σ_e^Q . This indicates that those SFGs have compact cores, but have larger r_e than typical quiescent galaxies. Thus, a threshold in Σ_1^Q is a more efficient selection criterion to identify compact SFGs and quiescent galaxies.

3.5. Relative distances from the SFR-MS and the quiescent structural relations: compaction and quenching

In this section we study the relative distributions of galaxies with respect to the SFR-MS and the $\Sigma_{e,1}^Q$ structural relations to identify candidate quenching galaxies as a function of redshift. Qualitatively, this analysis is similar to studying the distribution with respect to the SFR- and Σ - main sequences. However, using the $\Sigma_{e,1}^Q$ frames the selection around quiescent galaxies, searching for SFGs with similar structural properties to them.

3.5.1. Compact SFGs as progenitors of quiescent galaxies

As discussed in the previous section, the higher normalization of the quiescent Σ_e^Q and Σ_1^Q relations with respect to those of SFGs indicates that quenching is preceded by an increase in the surface density above a certain threshold. However, as shown in Figure 2, such characteristic density scales with stellar mass, challenging the simple notion of a *fixed* quenching threshold at a given surface density or stellar mass (e.g., Kauffmann et al. 2003; Franx et al. 2008). In turn, the most effective quiescent criterion is a selection with respect to the Σ_e^Q or Σ_1^Q sequences with stellar mass, i.e., a relative offset from the structural relations. Such relative selection includes fewer SFGs. However, there is always overlap with quiescent galaxies at every redshift. A possible interpretation, outlined in the previous section, is that those overlapping

SFGs acquire quiescent morphologies while they are still star-forming as a result of a compaction process, i.e., a structural transformation that increases the central density and Sérsic index, and reduces the size *before* quenching star-formation. Such an evolutionary sequence was confirmed in Barro et al. (2013, 2014a, hereafter B13) for SFGs at $z \sim 2$. In B13, the authors used a selection on specific SFR and relative distance to the quiescent size-mass relation to identify compact SFGs at $z \sim 2$, finding that those galaxies have similar sizes, Sérsic indices and spheroidal morphologies as the quiescent population.

Building on this idea, in this work we define *compact* SFGs as those SFGs ($\Delta\text{SFR}_{\text{MS}} > -0.7$ dex) found within the $\sim 2\times$ the scatter of the quiescent structural scaling relations at a given redshift, $\Delta\Sigma_{e,1}^Q \equiv \log \Sigma_{e,1} - \log \Sigma_{e,1}^Q(z) > -2\sigma(\log \Sigma^Q)$, where $\Sigma_{e,1}$ is either the central or effective mass density, and we use $2\sigma(\log \Sigma_e^Q) = 0.5$ dex and $2\sigma(\log \Sigma_1^Q) = 0.2$ dex, respectively. This definition differs from previous works where *compact* is an absolute term to identify the smallest galaxies at high- z ($r_e \lesssim 1$ kpc; e.g., Cassata et al. 2011, 2013). Here, *compact* is a *relative* term referring to the densest/smallest SFGs at every redshift. Panels A and B of Figure 7 illustrate the selection of compact SFGs in Σ_e and Σ_1 (dashed line). In the x-axis we add the zero-point at each redshift to illustrate the different time evolution in the normalization of these relations. Panel A shows also the *compactness* threshold of B13 (purple

Compaction – Quenching Sequence

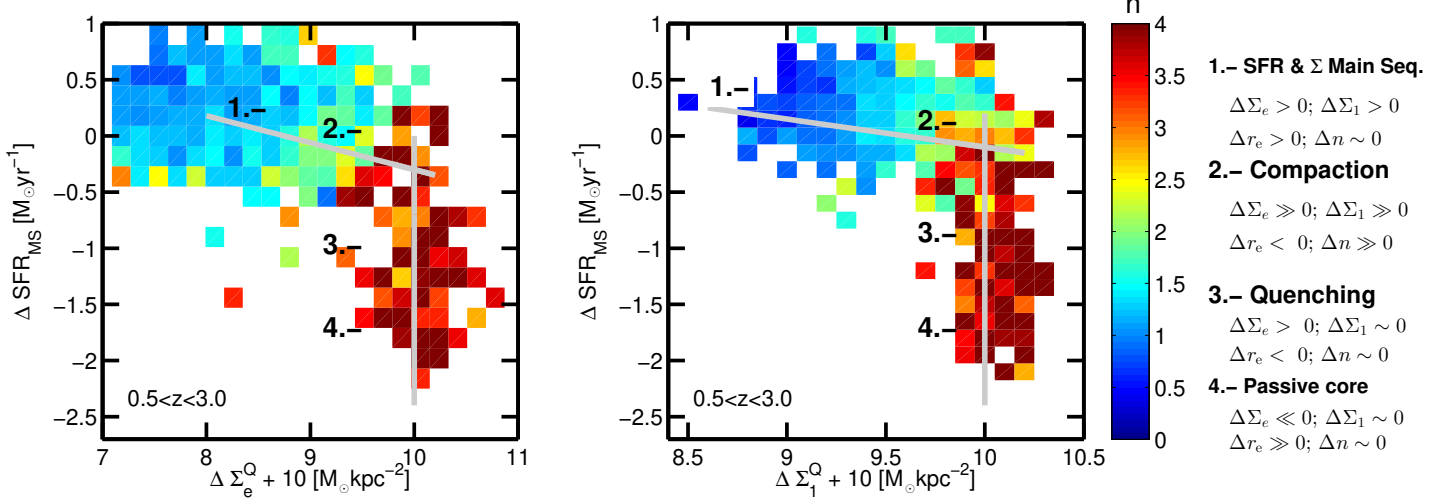


FIG. 8.— Stacked $\Delta\text{SFR-MS}$ vs. $\Delta\Sigma_e^Q$ (left) and $\Delta\Sigma_1^Q$ (right) for all massive galaxies at $0.5 < z < 3.0$, color coded by Sérsic index. The $\Delta\Sigma$ values are normalized at $\Sigma_e^Q = \Sigma_1^Q = 10$. The gray lines show the best-fit linear relations for SFGs and quiescent galaxies. The L-shape and the intrinsic scatter of these diagrams is independent of redshift, which suggests that all massive galaxies follow the same universal evolutionary path from star-forming to quiescent. The numbers and the legend on the right side summarize the main phases of such evolution: 1) The SFR and Σ -MS phase is a nearly horizontal track in which galaxies increase both their core mass and effective radius at relatively constant Sérsic (i.e., a disk growth); 2) Compaction is a phase of enhanced core growth, that increases the Sérsic index. Both 1) and 2) follow horizontal tracks, however, only compaction causes a substantial increase in n , pushing SFGs galaxies towards the knee of the relation. 3) Quenching is a nearly vertical track that indicates that the full shut down of star-formation happens at maximum Σ_e and Σ_1 . 4) In the passive core phase Σ_1 remains constant (or declines slowly due to dying stars), while Σ_e decreases faster due to size growth or new arrivals, causing a large evolution in the normalization of Σ_e^Q (Figure 7). The slight tilt of the Σ -MS to compaction phase indicates that the onset of quenching starts begins before reaching the maximum stellar density.

line), which, by definition, matches $\Delta\Sigma_e^Q < 0.5$ dex at $z \sim 1.8$. However, as the normalization of Σ_e^Q declines with time, a fixed selection threshold gets progressively fewer galaxies. In turn, $\Delta\text{SFR}_{\text{MS}} - \Delta\Sigma_e^Q$ is essentially a redshift-independent extension of the method to identify star-forming progenitors of quiescent galaxies.

The relative distributions of SFGs and quiescent galaxies in both panels of Figure 7 are very similar. By definition, both $\Delta\Sigma_1^Q$ and $\Delta\Sigma_e^Q$ select all quiescent galaxies within the typical scatter of the structural relations. A Σ_e selection exhibits a few more catastrophic outliers, most likely due to extreme values of the Sérsic also affecting the r_e (see e.g., van der Wel et al. 2012). Nonetheless, both Σ_e and Σ_1 identify the bulk of the quiescent population. The selection of compact SFGs is also largely consistent. However, Σ_1 selects $\sim 10 - 15\%$ more compact galaxies at each redshift. These compact SFGs in Σ_1 scattered outside the Σ_e selection have both dense centers and extended star-forming profiles, which leads an overall higher r_e in a single Sérsic fit (e.g., Bruce et al. 2012). Nonetheless, as discussed for example in Fang et al. (2013), these galaxies will eventually increase their Σ_e as the extended star-forming disk fades. Thus, they are bonafide quiescent progenitors. The lower efficiency of Σ_e for selecting compact SFGs is a result of r_e not being monotonic with time (i.e., r_e both increases and decreases with redshift).

In summary, Σ_1 is closer to a *clock* (it only increases), and it also exhibits a tighter scatter and a slower evolution the normalization, so we conclude that $\Delta\Sigma_1^Q$ is a more efficient criterion to identify compact SFGs. In fact, as shown in panel B of Figure 7, a single threshold of $\Sigma_1 - 0.65 \log(M_\star - 10.5) \gtrsim 9.5 \text{ M}_\odot/\text{kpc}^2$ identifies the

majority of compact SFGs and quiescent galaxies at redshifts $z > 0.5$. Hereafter, we will refer to compact SFGs as those selected in Σ_1 .

3.5.2. A universal compaction-quenching sequence

The remarkable similarity in the galaxy distributions of Figure 7 as a function of time suggest that the relative distance from the SFR-MS and $\Sigma_{e,1}^Q$ relations describes a universal evolutionary sequence for massive galaxies, which is independent of redshift. Figure 8 illustrates this sequence showing the stacked distribution in $\Delta\text{SFR}_{\text{MS}}$ vs. $\Delta\Sigma^Q$ for the redshift range $0.5 < z < 3.0$. The upside-down, L-shaped sequence summarizes the notion that forming a dense stellar core is a pre-requisite for quenching star-formation (Cheung et al. 2012, Bell et al. 2012; Fang et al. 2013). The color code in Sérsic index emphasizes that the evolution requires *both* the growth of a dense stellar core, and a structural transformation from an exponential (disk) profile to more a concentrated ($n \gtrsim 2$) Sérsic profile. Incidentally, Figure 8 also illustrates why the Sérsic index is a better quiescent indicator than a constant threshold in Σ_e , Σ_1 or velocity dispersion, σ (e.g., Bell et al. 2012).

In terms of the galaxy evolutionary paths discussed in § 3.4 the two branches of the L-shaped sequence describe two fundamental transitions from the Σ - and SFR-main sequences, respectively: compaction and quenching. The horizontal branch of SFGs represents constant evolution along the SFR-MS, but an eventual departure from the Σ -MS due to a compaction event. The Σ -MS describes the growth of an exponential disk ($n \sim 1$) due to in-situ star-formation, which increases Σ_1 , Σ_e and the overall size of the galaxy. Compaction involves a

stronger increase in Σ_1 and Σ_e , leading to a steeper mass profile ($n \gtrsim 2$) and a smaller r_e . The vertical branch shows that quenching (defined as $\Delta\text{SFR}_{\text{MS}} > -0.7$ dex) takes places at maximum central density in compact SFGs with similar morphologies to the quiescent population, i.e., compaction precedes the *full* shut down of star-formation. The slight tilt in the horizontal branch, $\Delta\text{SFR}_{\text{MS}} \sim -0.20\Delta\Sigma_1^{\text{Q}}$, $\Delta\text{SFR}_{\text{MS}} \sim -0.25\Delta\Sigma_e^{\text{Q}}$ (gray lines), however, suggests that while quenching is completed at maximum central density it starts some time before.

Following the interpretation of B13, we characterize the evolutionary pace along compaction-quenching path as declining from fast to slow as a function of time. The gradient in quenching speed arises naturally from the decline in sSFR with time (e.g., Speagle et al. 2014). Since $\Delta \log \Sigma_{1,e} \propto \Delta \log M \propto \text{sSFR}(z)$, the central densities increase more slowly with time. The larger SFR at high- z is associated with higher gas fractions (Tacconi et al. 2010; Tacconi et al. 2013), which are likely related with larger accretion rates from the dark matter haloes (Dekel et al. 2013; Dekel & Burkert 2014). Simple stability arguments predict that such gas rich galaxies are prone also to stronger gravitational instabilities, and thus favor more expedite compaction and quenching processes. In such case, the tilt in Figure 8, could be due to gas *starvation* after an instability-induced starburst, i.e., a wet-inflow that causes a peak in SFR at maximum gas density, and declines progressively with the gas supply, while the core mass increases (e.g., Feldmann & Mayer 2015; Zolotov et al. 2015). The truncation of the gas supply to the galaxy center can be caused by a combination of feedback (e.g., outflows) and stabilization of the disk due to the increasing central density (Martig et al. 2009).

At lower redshift, the smaller gas fractions and longer dynamical timescales suggest that compaction mechanisms become a mixture of weaker instabilities, which can still cause enhanced gas inflows or inward migration of stellar clumps (e.g., Dekel et al. 2009b; Bournaud et al. 2011; Genel et al. 2012), and *secular* processes (Kormendy & Kennicutt 2004) associated with torques and dynamical friction in the presence of bars and spiral arms. The latter play an important role increasing the central density in SFGs that already exhibit relatively quiescent centers, i.e., lacking enough star-formation to sustain the core growth required to reach Σ_1^{Q} (Wuyts et al. 2012, 2013; Lang et al. 2014; Bruce et al. 2014b,a). In those SFGs, quenching is also expected to be a slow process, related with gas consumption in the star-forming disk (fading; e.g., Fang et al. 2013; Tacchella et al. 2015). The slow quenching process depends also on additional mechanisms to prevent further gas accretion into the disk, e.g., virial shock heating in massive haloes (Croton et al. 2006; Dekel & Birnboim 2006) or AGN feedback (. As mentioned in the previous section, some of these SFGs are compact in Σ_1 but not in Σ_e . Therefore, the tilt in $\Delta\text{SFR}_{\text{MS}}$ vs. $\Delta\Sigma_e^{\text{Q}}$ can be caused by the size shrinkage (r_e) associated with fading rather than with an increase in their core mass.

3.5.3. Number density of compact SFGs and quiescent galaxies

The existence of a universal compaction-quenching diagram and the increasing number density of quiescent

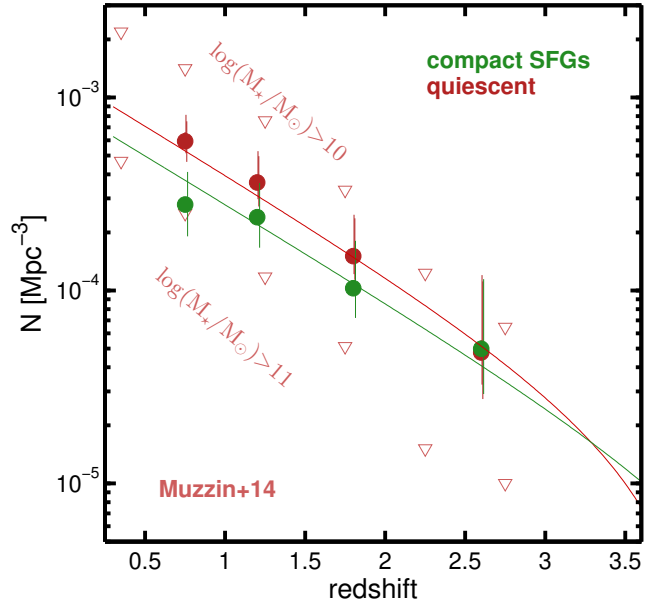


FIG. 9.— Redshift evolution of the number density of massive ($\log(M/M_{\odot}) > 10.3$) compact SFGs and quiescent galaxies. Compact SFGs are selected using the Σ_1^{Q} criterion. The red triangles indicate the evolution in the number density of quiescent galaxies in different mass ranges from Muzzin et al. (2013). The green and red lines show the best-fit evolutionary model to the observed number of compact SFGs and quiescent galaxies. The model is based on the assumption that quiescent galaxies are descendants of compact SFGs that have a characteristic quenching timescale λ^{Q} , but can also increase in number due to compaction events in more extended SFGs that have a frequency λ^{SFG} . This simple model that assumes a continuous replenishment of compact SFGs at every redshift can account for the observed evolution in the two populations.

galaxies as a function of time supports the idea that the L-shaped diagram is indeed an evolutionary sequence, i.e., compact SFGs in the knee of the relation are immediate progenitors of the quiescent galaxies at lower redshifts. Figure 9 shows the evolution in the number density of compact SFGs, selected using $\Delta\Sigma_1^{\text{Q}} > -0.2$, and all quiescent galaxies, regardless of their structural properties, since $z \sim 3$. The latter grows approximately as a power-law, $N^{\text{Q}} \sim 10^{-0.5(1+z)}$, in good agreement with previous results (e.g., Muzzin et al. 2013). Assuming that quiescent galaxies are descendants of compact SFGs at higher redshift, the number of quiescent galaxies is the cumulative distribution of quenching compact SFGs as a function of time. To quantify the relative numbers of these two populations we assume that the number density of compact SFGs also follows a power-law evolution as the result of 2 opposite processes that cause either an increase (due to compaction) or decrease (due to quenching) in their total number: $dN_{\text{SFG}}/dz = \lambda_{\text{C}}N_{\text{SFG}} + \lambda_{\text{Q}}N_{\text{SFG}}$. In this model, the evolution in the number of quiescent galaxies is proportional to the number of quenching SFGs, and thus inherit the power-law dependence: $dN^{\text{Q}}/dz = -\lambda_{\text{d}}N_{\text{SFG}} \sim -\lambda_{\text{Q}}10^{(\lambda_{\text{C}}+\lambda_{\text{Q}})(1+z)}$. There are two additional parameters which determine the initial number compact SFGs and quiescent galaxies, $N_{z_0}^{\text{SFG}}$ and $N_{z_0}^{\text{Q}}$. We set $N_{z_0}^{\text{Q}} = 0$ at $z_0 = 4$, and we fit the other 3 parameters to the observed number density of compact SFGs and quiescent galaxies,

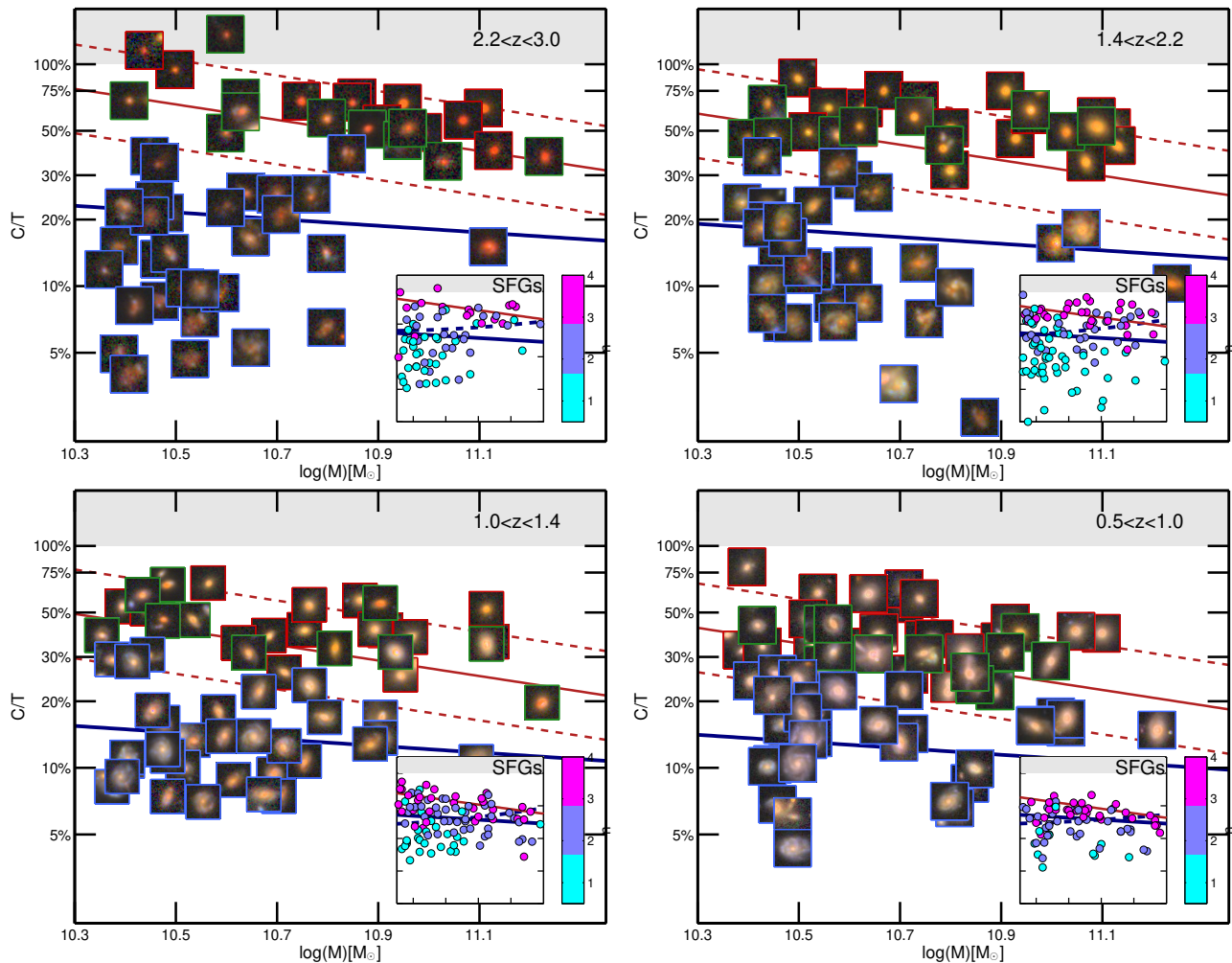


FIG. 10.— Core to total mass ratio (C/T) vs. stellar mass for a representative sub-sample of massive galaxies at different redshifts. The color composite ACS/WFC3 zJH images illustrate the evolution in the morphology of SFGs and quiescent galaxies as a function of time. The color of the border around the postage stamps indicate the location of the galaxy in the three regions of the compaction-quenching diagram (Figure 8). The solid blue and red lines indicate the best fit Σ_1 relations for SFG and quiescent galaxies at each redshift. The dashed lines indicate the typical width of the Σ_1^Q relation, which is the threshold used to select compact SFGs. The insets show the same diagram color coded by Sérsic index for all massive SFGs. SFGs evolving in the Σ -MS decrease their C/T with time as the disk component becomes more prominent (i.e., the disk grows faster than the core). Similarly, quiescent galaxies decrease their C/T with time as they grow larger stellar envelopes. However, SFGs that have a compaction event, experience a significant core growth relative to the total mass (increasing their C/T), moving upwards from the Σ -MS to the quiescent relation. The visual appearances of compact SFGs (green) are very similar to those of quiescent galaxies at all redshifts, but are most different from other SFGs only at high- z (see also Figure 11).

which yields $\lambda_i = 1.27 \pm 0.15$, $\lambda_d = -0.75 \pm 0.12$ and $N_{z0}^{\text{SFG}} = 5 \cdot 10^{-6} \text{ Mpc}^{-3}$. Thus, the characteristic quenching timescale for a compact SFG in units of redshift is $z_{1/2,Q} = \ln(10)/\ln(2)/\lambda_Q = 0.38$, which implies that the quenching time increases from $t_Q = 700 \text{ Myr}$ to 1.1 Gyr at $z = 3$ and $z = 1$. In spite of its simplicity, this model provides a more realistic approximation than previous assumptions that all compact SFGs form and quench in discrete intervals of time. In this case, the number densities vary continuously while preserving the evolutionary connection as a characteristic quenching time.

3.6. Galaxy morphologies in the universal compaction-quenching sequence

As discussed in § 3.5, the shape of the compaction-quenching sequence is independent of redshift. However, the evolutionary pace along the sequence declines with time as compaction, and most likely quenching, processes

become slower. Furthermore, the evolution in the normalization of Σ_e clearly indicates that the structural and morphological properties of galaxies in the sequence depend on the redshift.

Figure 10 illustrates the evolution in the visual appearances of SFGs and quiescent galaxies as a function of time in the core-to-total vs. mass diagram. The thumbnail frames are color coded according to the location of the galaxies in the 3 regions of the compaction-quenching diagram (Figure 8). Overall, the evolutionary tracks in this diagram follow decreasing trends in C/T for both SFGs (i.e., inside-out growth of a disk), and quiescent galaxies (i.e., stellar halo growth). Only SFGs experiencing a compaction event (from blue to green) follow a trend of increasing C/T . Note that, conceptually, C/T is similar to a *bulge*-to-total ratio. However, bulges can typically grow beyond a radius of 1 kpc, in fact, recent results indicate that both the bulge size and its mass

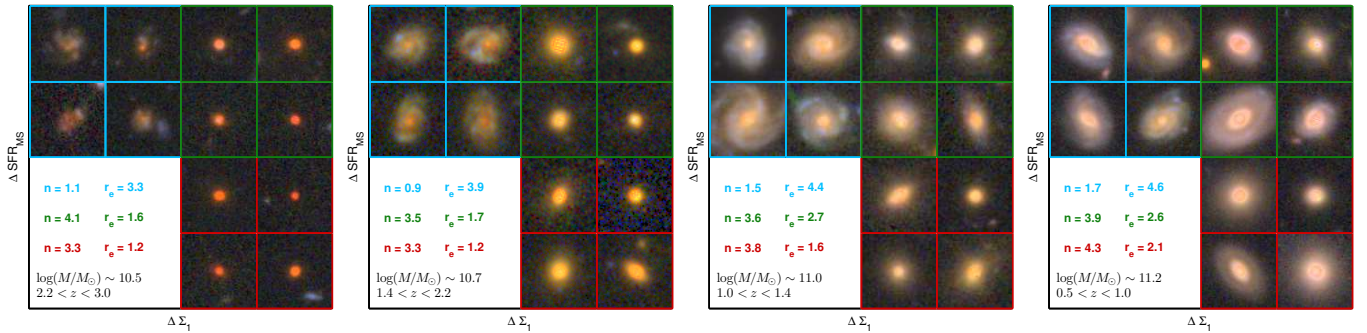


FIG. 11.— Postage stamps in the $\Delta\text{SFR}_{\text{MS}}-\Delta\Sigma_1^{\text{Q}}$ plane, showing galaxies in three different phases of the compaction-quenching sequence (see Figure 7): extended SFGs (blue), compact SFGs (green) and quiescent galaxies (red). Each panel shows galaxies with increasing stellar masses as a function of time (left to right) following the expected mass growth from $z = 3$ to $z = 0.5$ predicted by semi-analytic models. The numbers on the inset indicate the median n and r_e of the galaxies in each group. The evolutionary sequence, discussed in § 3.5.2, suggests that some SFGs grow along the Σ -MS from $z = 3$ to $z = 0.5$ (blue), while others experience a compaction event (green), departing from the Σ -MS. Compaction produces a steeper mass profile, resulting in a strong increase in Σ_1 and Σ_e . After compaction, galaxies quench (red), showing only minor changes in their structural and visual appearances relative to their compact SFG progenitors. The Σ -MS describes the growth of a disk, starting from a small, irregular morphology and becoming progressively more settled with time, increasing both its size and central density (bulge growth). The pre- and post-compaction appearances of SFGs at high- z are radically different, suggesting the action of a strongly dissipative process. However, at low- z , many compact SFGs exhibit disks, indicating that compaction affects mostly the central region of the galaxy. The overall appearance of quiescent galaxies evolves from “naked” to “clothed” cores (i.e., larger r_e at similar Σ_1). Such evolution is likely driven by size growth in quiescent galaxies formed at high- z , and the formation of new quiescent galaxies from compact SFGs with larger sizes.

correlate with the total mass of the galaxy, i.e., B/T increases with mass, as opposed to C/T (e.g., Lang et al. 2014). Qualitatively, the visual appearances agree with this evolution. The bulk of SFGs exhibit larger and more settled disks as a function of time, while also increasing their central densities. The steeper slope of Σ_1^{SF} seems clear in this diagram (dashed blue line), particularly at $z < 1$, where slow compaction processes push most SFGs above $C/T \gtrsim 10\%$. Quiescent galaxies also show larger (*puffed up*) appearances with time with values declining from $C/T \sim 60\%$ at $z = 2.6$ (“naked”-cores) to 35% and $z = 0.75$ (“clothed”-cores).

To further illustrate the change in visual appearances within an evolutionary path, Figure 11 shows images of galaxies with increasing stellar mass as a function of time in the 3 regions of the compaction-quenching sequence. The increase in stellar mass with redshift follows the average mass growth in galaxies with $\log(M/M_\odot) = 10.5$ at $z = 2.5$. There are several methods to estimate the typical stellar mass growth with redshift (e.g. van Dokkum et al. 2010; Patel et al. 2013; Marchesini et al. 2014). Here we adopt the evolutionary tracks of Moster et al. (2013) determined from semi-analytic models, with average mass growth of $\Delta M_\star = 0.7$ dex from $z = 2.5$ to $z = 0.75$. Since galaxies of a given mass can be in any of the three stages at a given redshift, we assume that at each redshift some SFGs remain in the left region (blue) growing along the Σ_1 -MS, others move rightward due to compaction (blue to green), and some compact SFGs quench downward after reaching a maximum central density (green to red).

The morphologies and visual appearances change strongly as a function of redshift: 1) at $z \gtrsim 1.4$, compaction involves a significant structural transformation going from irregular, clumpy SFGs to compact “naked” spheroids. Compact SFGs quench having almost identical morphologies than quiescent galaxies at those redshifts (see also Barro et al. 2014a). Extended SFGs in the Σ -MS (blue) increase their size, central density and total mass with time. However, as total mass grows faster than the core mass, their C/T decreases. By $z \lesssim 2$

these galaxies exhibit clear disk-like structures and distinct cores with redder colors (see also Wuyts et al. 2012; Lang et al. 2014; Tacchella et al. 2015). 2) at $z < 1.4$, extended SFGs show larger, more settled disks and similarly more massive cores. Compact SFGs and quiescent galaxies also have denser cores, but, in contrast with the high- z appearances, they exhibit diffuse extended components (some clearly star-forming). This suggests that the compaction process at lower redshift preserves the already existing disk structure. The evolution towards disk-like morphologies with progressively bigger cores eventually results in the prominence of disks with bulges among massive SFGs and quiescent galaxies at $z \gtrsim 1$ reported in previous works (e.g., Bundy et al. 2010; Bruce et al. 2012; Bruce et al. 2014a; Buitrago et al. 2013; McLure et al. 2013; Lang et al. 2014; Huertas-Company et al. 2015). As noted in previous works, however, the progenitor bias makes it nearly impossible to distinguish between puffed-up, older galaxies and newly quenched galaxies with larger sizes attending only to their morphologies.

4. SUMMARY

We analyze the star-formation and structural properties of massive galaxies in the CANDELS/GOODS-S field to study the relation between stellar mass and structural growth, and the role of the latter in the quenching of star-formation since $z \sim 3$. We characterize the structural properties as a function of redshift by studying the correlations in the mass surface density within the effective radius, Σ_e , and within the central 1 kpc, Σ_1 , vs. stellar mass. Σ_1 traces the stellar mass growth in the galaxy core, and thus it is close to the concept of a cosmic clock (i.e., it increases with time). Σ_e , however, depends on the relative balance between stellar mass and size growth, and thus it exhibits positive and negative fluctuations.

We find that SFGs and quiescent galaxies follow clear and distinct correlations in Σ_e and Σ_1 vs. stellar mass since $z \sim 3$. These correlations are well-described by lin-

ear relations in log-log space. The slopes and scatter of these relations are relatively constant with time, while their normalizations decline (see Table 1). The scatter in the Σ_1 structural relations is $\sim 2\times$ tighter than in the Σ_e relations for both SFGs and quiescent galaxies. For SFGs, the normalizations in Σ_e and Σ_1 decrease by less than factor of ~ 2 from $z = 3$ to $z = 0.5$. For quiescent galaxies, the decline in Σ_e is $5\times$ larger than in Σ_1 (~ 0.3 dex vs. ~ 1 dex, respectively). The differential evolution of the normalization in Σ_e^Q and Σ_1^Q is inconsistent with a simple minor merger scenario in which the core mass remains constant while the size increases. However, the normalizations at redshifts $z = 3$ to $z = 0.5$ agree well with one another if the mass profiles of quiescent galaxies follow a single Sérsic with $n \sim 4$. Thus the large increase with time in the size of quiescent galaxies is consistent with just modest decline in Σ_1 at constant Sérsic. Such decline can be caused by the formation of new quiescent galaxies with lower density cores or mass loss due to passive evolution in the already existing population.

Based on the slow decline in the normalizations of the structural relations for SFGs, we speculate that these galaxies follow evolutionary paths *along* the $\Sigma_{e,1}$ correlations. We define these paths as the Σ main sequence, following the paradigm of the SFR-MS as a smooth phase of stellar and structural growth (e.g., Elbaz et al. 2011; Rodighiero et al. 2011). The evolution in the Σ -MS is consistent with the inside-out growth of an exponential disk due to in-situ star-formation, i.e., an increase in both the core mass and the overall size of the galaxy.

At every mass and redshift, quiescent galaxies have steeper mass profiles (higher Sérsic) and higher surface densities than SFGs. This implies that growing a dense stellar core is a pre-requisite for quenching star-formation (see also, Cheung et al. 2012, Bell et al. 2012; Fang et al. 2013; van Dokkum et al. 2014). Thus, the immediate star-forming progenitors of quiescent galaxies must experience a phase of stronger core-growth, relative to the Σ -MS. We define this phase(s) of fast increase in Σ_1 , Σ_e and n as *compaction*. The compaction phase is typically associated with dissipational processes ranging from major mergers (Hopkins et al. 2006; Hopkins et al. 2008), to violent gravitational instabilities (Dekel et al. 2009a; Dekel & Burkert 2014; Ceverino et al. 2010), and weaker *secular* instabilities (e.g., bars and spiral arms; Kormendy & Kennicutt 2004). The evolutionary tracks of massive SFGs in recent hydrodynamical simulations exhibit an excellent agreement with the Σ -MS/compaction scenario (Ceverino et al. 2015; Zolotov et al. 2015). The simulations suggest that SFGs depart from a steady-state evolution along the Σ -MS as a result of dissipational compaction events triggered by intense episodes of gas inflow. The strength and duration of these events declines with time following a decline in the gas reservoirs of SFGs (Dekel et al. 2013).

We find that the 2D distribution of SFGs and quiescent galaxies relative to the SFR-MS and the quiescent structural relations, $\Delta\Sigma_{\text{MS}} - \Delta\Sigma_{e,1}^Q$, exhibits a universal L-shape that is independent of redshift (Figure 7). Each branch of this distribution describes a fundamental transition in the evolution of SFGs, namely: compaction and quenching. The horizontal branch describes

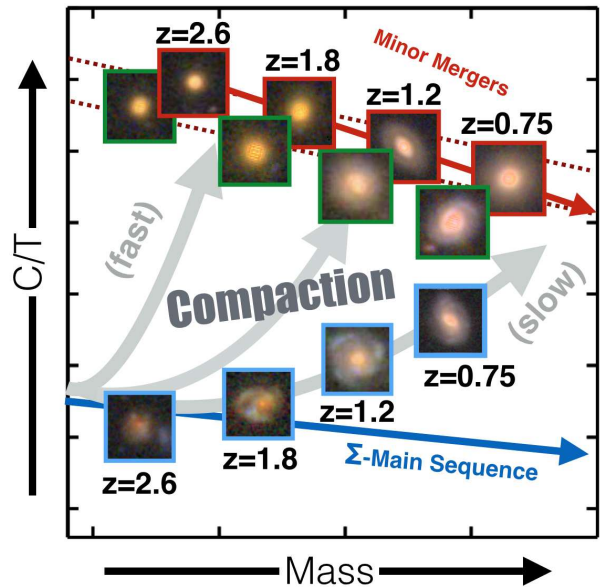


FIG. 12.— Structural evolutionary path of massive galaxies since $z \sim 3$ in terms of their core ($r < 1$ kpc) to total mass (C/T) vs. stellar mass. The typical SFG follows a structural “main sequence” that describes the inside-out growth of a disk (blue-framed images), i.e., increasing its stellar mass and r_e as does its central density (bulge growth). Prior to quenching, SFGs experience a dissipative compaction phase of enhanced core growth (green-framed images) fueled by the inward migration of gas into the central region. Compaction events are strongest at high- z , due to higher gas fractions, forming extremely compact SFGs on very short timescales. At low- z the strength of compaction diminishes, the core growth becomes slower and it preserves the underlying disk structure. Newly quenched galaxies at each redshift (red-framed images) are direct descendants of compact SFGs, which shut down star-formation after forming a dense stellar core with no further structural changes. Quiescent galaxies grow an extended stellar halo due to minor merging, decreasing their C/T . Quenching timescales depend on the strength of the compaction process, which drives a major gas consumption event. Thus, qualitatively, quenching follows the fast shut-down of a compact core at high- z and the slower fading of a star-forming disk at low- z .

the growth in size and core mass of a SFG along the Σ -MS, followed by a compaction event that causes a strong increase in surface density and Sérsic index. Compaction marks the departure from the Σ -MS towards the knee of the L-shaped distribution. The vertical branch describes the quenching of star-formation at maximum core and effective surface density. The latter implies that the formation of a dense core precedes the quenching of star-formation. Therefore, *compact* SFGs in the knee of the L-diagram at every redshift are the most likely progenitors of quiescent galaxies at lower- z . Owing to the mild decline in the normalization of the Σ_1^Q relation with time, a constant threshold of $\Sigma_1^Q \equiv \Sigma_1 - 0.65 \log(M_* - 10.5) \gtrsim 9.5$ identifies compact SFGs at any redshift $z > 0.5$.

Although the L-shape of the compaction-quenching sequence is independent of redshift, the rate of growth along the sequence and the strength of the transformation processes declines with time following the similar decline in the overall SFR (e.g., Whitaker et al. 2014; Speagle et al. 2014). As a result, the morphologies of galaxies in each region of the sequence are substantially different with time. Figure 12 describes qualitatively the change in morphologies and core-to-total ratios for galaxies following fast-to-slow evolutionary paths in the

compaction-quenching sequence as a function of time.

At high- z , SFGs have larger gas reservoirs and thus follow a faster mass growth (Tacconi et al. 2010; Tacconi et al. 2013). Those SFGs are also prone to stronger gravitational instabilities and expedited compaction processes capable of transforming SFGs with clumpy, irregular morphologies into compact SFGs with spheroid-like morphologies, high Sérsic and high core-to-total ratios (Dekel & Burkert 2014; Wellons et al. 2014; Ceverino et al. 2015; Zolotov et al. 2015). I.e., “naked” star-forming cores, which appear to quench fast turning into compact quiescent galaxies (Bezanson et al. 2013; Onodera et al. 2014; Belli et al. 2014b; Barro et al. 2015) with similar masses and structural properties.

At low- z , SFGs have lower gas fractions and SFRs, which implies a slower mass growth and weaker gravitational instabilities. This is consistent with SFGs having more settled, disk-like morphologies, larger sizes, and progressively denser cores (see also, Bruce et al. 2012; Lang et al. 2014; Tacchella et al. 2015). As opposed to high- z , the similar morphologies of compact SFGs (green-

framed images) and SFGs in the Σ -MS (blue-framed images) suggests that compaction at low- z causes an enhanced core growth, increasing C/T within an already existing disk. Many SFGs at low- z exhibit blue disks and red cores, suggesting that quenching star-formation (in the whole galaxy) is a slower process that causes also minor changes in their appearances due to disk-fading.

ACKNOWLEDGMENTS

Support for Program number HST-GO-12060 was provided by NASA through a grant from the Space Telescope Science Institute, which is operated by the Association of Universities for Research in Astronomy, Incorporated, under NASA contract NAS5-26555. GB acknowledges support from NSF grant AST-08-08133. PGP-G acknowledges support from grant AYA2012-31277. This work has made use of the Rainbow Cosmological Surveys Database, which is operated by the Universidad Complutense de Madrid (UCM), partnered with the University of California Observatories at Santa Cruz (UCO/Lick,UCSC). This work was partly supported, by MINECO grant AYA2012-32295. FL acknowledges support from NSFC grant 11573017

REFERENCES

- Barro, G., Faber, S. M., Dekel, A., et al. 2015, ArXiv e-prints
 Barro, G., Faber, S. M., Pérez-González, P. G., et al. 2013, *ApJ*, 765, 104
 —. 2014a, *ApJ*, 791, 52
 Barro, G., Pérez-González, P. G., Gallego, J., et al. 2011, *ApJS*, 193, 30
 Barro, G., Trump, J. R., Koo, D. C., et al. 2014b, ArXiv e-prints
 Bell, E. F. 2008, *ApJ*, 682, 355
 Bell, E. F., Papovich, C., Wolf, C., et al. 2005, *ApJ*, 625, 23
 Bell, E. F., van der Wel, A., Papovich, C., et al. 2012, *ApJ*, 753, 167
 Belli, S., Newman, A. B., & Ellis, R. S. 2014a, *ApJ*, 783, 117
 Belli, S., Newman, A. B., Ellis, R. S., & Konidaris, N. P. 2014b, *ApJ*, 788, L29
 Bezanson, R., van Dokkum, P., van de Sande, J., Franx, M., & Kriek, M. 2013, *ApJ*, 764, L8
 Bezanson, R., van Dokkum, P. G., Tal, T., et al. 2009, *ApJ*, 697, 1290
 Bournaud, F., Chapon, D., Teyssier, R., et al. 2011, *ApJ*, 730, 4
 Bouwens, R. J., Illingworth, G. D., Oesch, P. A., et al. 2010, *ApJ*, 708, L69
 Brammer, G. B., van Dokkum, P. G., & Coppi, P. 2008, *ApJ*, 686, 1503
 Brammer, G. B., Whitaker, K. E., van Dokkum, P. G., et al. 2011, *ApJ*, 739, 24
 Bruce, V. A., Dunlop, J. S., Cirasuolo, M., et al. 2012, ArXiv e-prints
 Bruce, V. A., Dunlop, J. S., McLure, R. J., et al. 2014a, *MNRAS*, 444, 1660
 —. 2014b, *MNRAS*, 444, 1001
 Bruzual, G. & Charlot, S. 2003, *MNRAS*, 344, 1000
 Buitrago, F., Trujillo, I., Conselice, C. J., et al. 2008, ArXiv e-prints
 Buitrago, F., Trujillo, I., Conselice, C. J., & Häußler, B. 2013, *MNRAS*, 428, 1460
 Bundy, K., Scarlata, C., Carollo, C. M., et al. 2010, *ApJ*, 719, 1969
 Calzetti, D., Armus, L., Bohlin, R. C., et al. 2000, *ApJ*, 533, 682
 Carollo, C. M., Bschorr, T. J., Renzini, A., et al. 2013, *ApJ*, 773, 112
 Cassata, P., Giavalisco, M., Guo, Y., et al. 2011, *ApJ*, 743, 96
 Cassata, P., Giavalisco, M., Williams, C. C., et al. 2013, *ApJ*, 775, 106
 Ceverino, D., Dekel, A., & Bournaud, F. 2010, *MNRAS*, 404, 2151
 Ceverino, D., Dekel, A., Tweed, D., & Primack, J. 2015, *MNRAS*, 447, 3291
 Ceverino, D., Klypin, A., Klimek, E. S., et al. 2014, *MNRAS*, 442, 1545
 Chabrier, G. 2003, *PASP*, 115, 763
 Chary, R. & Elbaz, D. 2001, *ApJ*, 556, 562
 Cheung, E., Faber, S. M., Koo, D. C., et al. 2012, ArXiv e-prints
 Croton, D. J., Springel, V., White, S. D. M., et al. 2006, *MNRAS*, 365, 11
 Daddi, E., Bournaud, F., Walter, F., et al. 2010, *ApJ*, 713, 686
 Damjanov, I., Abraham, R. G., Glazebrook, K., et al. 2011, *ApJ*, 739, L44
 Damjanov, I., McCarthy, P. J., Abraham, R. G., et al. 2009, *ApJ*, 695, 101
 Dekel, A. & Birnboim, Y. 2006, *MNRAS*, 368, 2
 Dekel, A., Birnboim, Y., Engel, G., et al. 2009a, *Nature*, 457, 451
 Dekel, A. & Burkert, A. 2014, *MNRAS*, 438, 1870
 Dekel, A., Sari, R., & Ceverino, D. 2009b, *ApJ*, 703, 785
 Dekel, A., Zolotov, A., Tweed, D., et al. 2013, *MNRAS*, 435, 999
 Elbaz, D., Daddi, E., Le Borgne, D., et al. 2007, *A&A*, 468, 33
 Elbaz, D., Dickinson, M., Hwang, H. S., et al. 2011, *A&A*, 533, A119
 Elmegreen, B. G., Bournaud, F., & Elmegreen, D. M. 2008, *ApJ*, 688, 67
 Elmegreen, D. M., Elmegreen, B. G., & Sheets, C. M. 2004, *ApJ*, 603, 74
 Faber, S. M. & Jackson, R. E. 1976, *ApJ*, 204, 668
 Fang, J. J., Faber, S. M., Koo, D. C., & Dekel, A. 2013, *ApJ*, 776, 63
 Feldmann, R. & Mayer, L. 2015, *MNRAS*, 446, 1939
 Franx, M., van Dokkum, P. G., Schreiber, N. M. F., et al. 2008, *ApJ*, 688, 770
 Genel, S., Naab, T., Genzel, R., et al. 2012, *ApJ*, 745, 11
 Genel, S., Vogelsberger, M., Springel, V., et al. 2014, *MNRAS*, 445, 175
 Genzel, R., Burkert, A., Bouché, N., et al. 2008, *ApJ*, 687, 59
 Giavalisco, M., Ferguson, H. C., Koekemoer, A. M., et al. 2004, *ApJ*, 600, L93
 Graham, A. W., Driver, S. P., Petrosian, V., et al. 2005, *AJ*, 130, 1535
 Grogin, N. A., Kocevski, D. D., Faber, S. M., et al. 2011, *ApJS*, 197, 35
 Guo, Y., Ferguson, H. C., Bell, E. F., et al. 2015, *ApJ*, 800, 39
 Guo, Y., Ferguson, H. C., Giavalisco, M., et al. 2013, *ApJS*, 207, 24
 Guo, Y., Giavalisco, M., Cassata, P., et al. 2012, *ApJ*, 749, 149
 Hopkins, P. F., Bundy, K., Murray, N., et al. 2009, *MNRAS*, 398, 898
 Hopkins, P. F., Hernquist, L., Cox, T. J., et al. 2006, *ApJS*, 163, 1
 Hopkins, P. F., Hernquist, L., Cox, T. J., & Keres, D. 2008, *ApJS*, 175, 356
 Kauffmann, G., Heckman, T. M., Tremonti, C., et al. 2003, *MNRAS*, 346, 1055
 Kennicutt, Jr., R. C. 1998, *ARA&A*, 36, 189
 Koekemoer, A. M., Faber, S. M., Ferguson, H. C., et al. 2011, *ApJS*, 197, 36
 Kormendy, J. & Kennicutt, Jr., R. C. 2004, *ARA&A*, 42, 603
 Kriek, M., van Dokkum, P. G., Franx, M., Illingworth, G. D., & Magee, D. K. 2009a, *ApJ*, 705, L71

- Kriek, M., van Dokkum, P. G., Labbé, I., et al. 2009b, *ApJ*, 700, 221
- Laidler, V. G., Grogan, N., Clubb, K., et al. 2006, in *Astronomical Society of the Pacific Conference Series*, Vol. 351, *Astronomical Data Analysis Software and Systems XV*, ed. C. Gabriel, C. Arviset, D. Ponz, & S. Enrique, 228
- Lang, P., Wuyts, S., Somerville, R. S., et al. 2014, *ApJ*, 788, 11
- Law, D. R., Steidel, C. C., Shapley, A. E., et al. 2012, *ApJ*, 745, 85
- Liu, F. S., Guo, Y., Koo, D. C., et al. 2013, *ApJ*, 769, 147
- López-Sanjuan, C., Le Fèvre, O., Ilbert, O., et al. 2012, *ArXiv e-prints*
- Magdis, G. E., Rigopoulou, D., Huang, J.-S., & Fazio, G. G. 2010, *MNRAS*, 401, 1521
- Marchesini, D., Muzzin, A., Stefanon, M., et al. 2014, *ApJ*, 794, 65
- Martig, M., Bournaud, F., Teyssier, R., & Dekel, A. 2009, *ApJ*, 707, 250
- McGrath, E. J., Stockton, A., Canalizo, G., Iye, M., & Maihara, T. 2008, *ApJ*, 682, 303
- McLure, R. J., Pearce, H. J., Dunlop, J. S., et al. 2013, *MNRAS*, 428, 1088
- Mosleh, M., Williams, R. J., Franx, M., et al. 2012, *ApJ*, 756, L12
- Moster, B. P., Naab, T., & White, S. D. M. 2013, *MNRAS*, 428, 3121
- Muzzin, A., Marchesini, D., Stefanon, M., et al. 2013, *ArXiv e-prints*
- Nelson, E., van Dokkum, P., Franx, M., et al. 2014, *Nature*, 513, 394
- Nelson, E. J., van Dokkum, P. G., Brammer, G., et al. 2012, *ApJ*, 747, L28
- Nelson, E. J., van Dokkum, P. G., Momcheva, I., et al. 2013, *ApJ*, 763, L16
- Newman, A. B., Ellis, R. S., Bundy, K., & Treu, T. 2012, *ApJ*, 746, 162
- Noeske, K. G., Weiner, B. J., Faber, S. M., et al. 2007, *ApJ*, 660, L43
- Onodera, M., Carollo, C. M., Renzini, A., et al. 2014, *ArXiv e-prints*
- Oser, L., Naab, T., Ostriker, J. P., & Johansson, P. H. 2012, *ApJ*, 744, 63
- Pannella, M., Carilli, C. L., Daddi, E., et al. 2009, *ApJ*, 698, L116
- Pannella, M., Elbaz, D., Daddi, E., et al. 2014, *ArXiv e-prints*
- Patel, S. G., van Dokkum, P. G., Franx, M., et al. 2013, *ArXiv e-prints*
- Peng, C. Y., Ho, L. C., Impey, C. D., & Rix, H.-W. 2002, *AJ*, 124, 266
- Peng, Y.-j., Lilly, S. J., Kovač, K., et al. 2010, *ApJ*, 721, 193
- Poggianti, B. M., Moretti, A., Calvi, R., et al. 2013, *ApJ*, 777, 125
- Porter, L. A., Somerville, R. S., Primack, J. R., & Johansson, P. H. 2014, *MNRAS*, 444, 942
- Rodighiero, G., Cimatti, A., Gruppioni, C., et al. 2010, *A&A*, 518, L25
- Rodighiero, G., Daddi, E., Baronchelli, I., et al. 2011, *ApJ*, 739, L40
- Salim, S., Rich, R. M., Charlot, S., et al. 2007, *ApJS*, 173, 267
- Santini, P., Ferguson, H. C., Fontana, A., et al. 2015, *ApJ*, 801, 97
- Schiminovich, D., Wyder, T. K., Martin, D. C., et al. 2007, *ApJS*, 173, 315
- Schreiber, C., Pannella, M., Elbaz, D., et al. 2015, *A&A*, 575, A74
- Sérsic, J. L. 1963, *Boletín de la Asociación Argentina de Astronomía La Plata Argentina*, 6, 41
- Speagle, J. S., Steinhardt, C. L., Capak, P. L., & Silverman, J. D. 2014, *ApJS*, 214, 15
- Stefanon, M., Marchesini, D., Rudnick, G. H., Brammer, G. B., & Whitaker, K. E. 2013, *ApJ*, 768, 92
- Szomoru, D., Franx, M., Bouwens, R. J., et al. 2011, *ApJ*, 735, L22
- Szomoru, D., Franx, M., & van Dokkum, P. G. 2012, *ApJ*, 749, 121
- Tacchella, S., Carollo, C. M., Renzini, A., et al. 2015, *Science*, 348, 314
- Tacconi, L. J., Genzel, R., Neri, R., et al. 2010, *Nature*, 463, 781
- Tacconi, L. J., Neri, R., Genzel, R., et al. 2013, *ApJ*, 768, 74
- Tomczak, A. R., Quadri, R. F., Tran, K.-V. H., et al. 2013, *ArXiv e-prints*
- van de Sande, J., Kriek, M., Franx, M., et al. 2013, *ApJ*, 771, 85
- van der Wel, A., Bell, E. F., Häussler, B., et al. 2012, *ApJS*, 203, 24
- van der Wel, A., Franx, M., van Dokkum, P. G., et al. 2014, *ApJ*, 788, 28
- van der Wel, A., Rix, H.-W., Wuyts, S., et al. 2011, *ApJ*, 730, 38
- van Dokkum, P. G., Bezanson, R., van der Wel, A., et al. 2014, *ApJ*, 791, 45
- van Dokkum, P. G., Nelson, E. J., Franx, M., et al. 2015, *ArXiv e-prints*
- van Dokkum, P. G., Whitaker, K. E., Brammer, G., et al. 2010, *ApJ*, 709, 1018
- Wellons, S., Torrey, P., Ma, C.-P., et al. 2014, *ArXiv e-prints*
- Whitaker, K. E., Franx, M., Leja, J., et al. 2014, *ApJ*, 795, 104
- Whitaker, K. E., van Dokkum, P. G., Brammer, G., & Franx, M. 2012, *ApJ*, 754, L29
- Whitaker, K. E., van Dokkum, P. G., Brammer, G., et al. 2013, *ArXiv e-prints*
- Williams, C. C., Giavalisco, M., Cassata, P., et al. 2013, *ArXiv e-prints*
- Williams, R. J., Quadri, R. F., Franx, M., et al. 2010, *ApJ*, 713, 738
- Woo, J., Dekel, A., Faber, S. M., & Koo, D. C. 2015, *MNRAS*, 448, 237
- Wuyts, S., Förster Schreiber, N. M., Genzel, R., et al. 2012, *ApJ*, 753, 114
- Wuyts, S., Förster Schreiber, N. M., Lutz, D., et al. 2011a, *ApJ*, 738, 106
- Wuyts, S., Förster Schreiber, N. M., Nelson, E. J., et al. 2013, *ApJ*, 779, 135
- Wuyts, S., Förster Schreiber, N. M., van der Wel, A., et al. 2011b, *ApJ*, 742, 96
- Zolotov, A., Dekel, A., Mandelker, N., et al. 2015, *ArXiv e-prints*